CrossMark

Local Discontinuous Galerkin Methods for the μ-Camassa–Holm and μ-Degasperis–Procesi Equations

Chao Zhang[1] · Yan Xu[1] · Yinhua Xia[1]

Abstract

In this paper, we develop and analyze a series of conservative and dissipative local discontinuous Galerkin (LDG) methods for the μ-Camassa–Holm (μCH) and μ-Degasperis–Procesi (μDP) equations. The conservative schemes for both two equations can preserve discrete versions of their own first two Hamiltonian invariants, while the dissipative ones guarantee the corresponding stability. The error estimates of both LDG schemes for the μCH equation are given. Comparing with the error estimates for the Camassa–Holm equation, some important tools are used to handle the unexpected terms caused by its particular Hamiltonian invariants. Moreover, a priori error estimates of two LDG schemes for the μDP equation are also proven in detail. Numerical experiments for both equations in different circumstances are provided to illustrate the accuracy and capability of these schemes and give some comparisons about their performance on simulations.

1 Introduction

We introduce and study the local discontinuous Galerkin (LDG) methods to approximate the μ-Camassa–Holm (μCH) equation

$$\mu(u)_t - u_{xxt} + 2\mu(u)u_x = 2u_x u_{xx} + uu_{xxx}, \tag{1.1}$$

✉ Yinhua Xia
   yhxia@ustc.edu.cn

   Chao Zhang
   zc56@mail.ustc.edu.cn

   Yan Xu
   yxu@ustc.edu.cn

[1] School of Mathematical Sciences, University of Science and Technology of China, Hefei 230026, Anhui, People's Republic of China

and the μ-Degasperis–Procesi (μDP) equation

$$\mu(u)_t - u_{xxt} + 3\mu(u)u_x = 3u_x u_{xx} + uu_{xxx}. \tag{1.2}$$

In fact, the μCH and μDP equations are the cases $\lambda = 2$ and $\lambda = 3$, respectively, of the following family of equations

$$\mu(u)_t - u_{xxt} + \lambda\mu(u)u_x = \lambda u_x u_{xx} + uu_{xxx}, \qquad \lambda \in \mathbb{Z}, \tag{1.3}$$

which is a corresponding μ-version of the family of equations defined as follows

$$u_t - u_{xxt} + (\lambda + 1)uu_x = \lambda u_x u_{xx} + uu_{xxx}, \qquad \lambda \in \mathbb{Z}, \tag{1.4}$$

that consists of the well known Camassa–Holm (CH) and Degasperis–Procesi (DP) equations with respective choices $\lambda = 2$ and $\lambda = 3$.

The μCH equation (1.1) originally derived and studied in [10] attracts a lot of attention. The variable $u(x, t)$ is a time-dependent function on the unit circle $\mathcal{S}^1 = \mathbb{R}/\mathbb{Z}$ and $\mu(u) = \int_{\mathcal{S}^1} u\,dx$ denotes its mean. In [10], the authors generalize that the μCH equation can be regarded as a natural generalization of the rotator equation in some sense and can also describe the geodesic flow endowed with the H_μ^1-inner product $(\cdot, \cdot)_\mu$ and associated H_μ^1-norm $\|\cdot\|_\mu$ as defined in [4]

$$(u, v)_\mu := \mu(u)\mu(v) + \int_{\mathcal{S}^1} u_x v_x dx, \tag{1.5}$$

$$\|u\|_\mu := \sqrt{(u, u)_\mu} = \sqrt{\mu(u)^2 + \int_{\mathcal{S}^1} u_x^2 dx}. \tag{1.6}$$

The closest relative of the μCH equation should be the Camassa–Holm equation

$$u_t - u_{xxt} + 3uu_x = 2u_x u_{xx} + uu_{xxx}, \tag{1.7}$$

which is a completely integrable system with the bi-Hamiltonian structure and can be viewed as a shallow water approximation. In [20], Xu and Shu developed a high-order accuracy and stable LDG method to solve the Camassa–Holm equation (1.7). The L^2 stability of their LDG method to CH equation is given, and a detailed error estimate for the scheme is also proven. Some efficient numerical experiments have validated their scheme and illustrated that the LDG methods have a good potential in solving these kinds of nonlinear equations. Our numerical schemes and main framework are inspired greatly by their contributions. Besides, another invariant preserving DG method for CH equation presented in [12] also give us some useful hints in designing conservative schemes for the μCH equation.

Based on the study from [4,10,11], we know that the μCH equation is also a completely integrable system with the bi-Hamiltonian structure and hence it has an infinite number of conservation laws. The first two invariants of the μCH equation described by

$$E_0(u) = \int_{\mathcal{S}^1} u\,dx, \qquad E_1(u) = \mu(u)^2 + \int_{\mathcal{S}^1} u_x^2 dx, \tag{1.8}$$

illustrate that, on the unit circle $\mathcal{S}^1$, the mean of any solution u and the H_μ^1-norm of u defined in (1.6) are both conservative in the time evolution. These properties enlighten us to design a conservative numerical scheme preserving the discrete counterpart of these conservation laws. A conservative scheme, together with a dissipative one, for the μCH equation are designed and analyzed in the present paper. Owing to the term $2\mu(u)u_x$ in the μCH equation (1.1), which is in fact a linearization of the analogue term $3uu_x$ in CH equation (1.7), the

subtle difference between the conservative and dissipative LDG schemes only exists in the choice of numerical flux for this term. For high order schemes, we will see that there is no qualitative distinction between these two schemes in numerical experiments. Owing to the really analogous structures and attributes of the μCH equation and CH equation, we will give the error estimates of the semi-discrete LDG schemes for the μCH equation by following the ideas and procedures of error estimates in [20] and applying some important tools to handle the unexpected terms, such as the Poincaré-Friedrichs inequality for discontinuous piecewise polynomials and the relationship between the auxiliary variables of the LDG methods.

As to the μDP equation (1.2), the notations $u(x, t)$ and $\mu(u)$ have the same meanings as in the μCH equation (1.1). Formally, the μDP equation can be described as an evolution equation on the space of tensor densities over the Lie algebra of smooth vector fields on the circle. The μDP equation is an extensive study of the well-known Degasperis–Procesi equation

$$u_t - u_{xxt} + 4uu_x = 3u_x u_{xx} + uu_{xxx}, \tag{1.9}$$

which has a similar form to the CH equation. Otherwise the DP equation truly possesses specific features, and one of them is that it admits not only peaked solutions but also shock waves. Xu and Shu in [24] first proposed two provable stable LDG schemes to simulate this DP equation. In their work, the L^2 stability for general solutions and total variation stability for piecewise constant case are both given. Motivated by the stability analysis in [24], high order methods such as the Fourier spectral methods [16] and weighted essentially non-oscillatory (WENO) schemes [17] for the DP equation have also been developed. The idea of constructing the L^2 stable scheme for the DP equation is also an important guideline to design the numerical method for the μDP equation.

By the work for the μDP equation in [11], we know the facts: analogous to the μCH equation, it is also a completely integrable system with a bi-Hamiltonian form and has an infinite number of conservation laws. Here we also list the first two conserved invariants

$$H_0(u) = \int_{\mathcal{S}^1} u dx, \qquad H_1(u) = \int_{\mathcal{S}^1} u^2 dx. \tag{1.10}$$

This indicates that the mean and L^2-norm of numerical solutions to the μDP equation keep conserved in the time evolution, which motivates us to design L^2 stable LDG schemes for the μDP equation. For this purpose, we choose another equivalent form of the μDP equation (1.2)

$$u_t + uu_x + 3\mu(u)(A_\mu^{-1}u)_x = 0, \tag{1.11}$$

where A_μ is an invertible linear operator defined as $A_\mu(u) = \mu(u) - u_{xx}$. Equation (1.11) is a consequence by applying A_μ^{-1} to both sides of (1.2), and the detailed derivation is given in "Appendix A.1". We will design and analyze two different schemes for the μDP equation. One scheme is conservative, which preserves the mean and L^2 energy of solutions to this nonlinear equation; another one is dissipative that still preserves $H_0(u)$ and just keeps the L^2 stability of numerical solutions. There is a relatively large difference between these two schemes due to the choices of numerical fluxes. The global L^2 projection, to deal with the central fluxes and thus requiring special assumptions over the parity of the degree of polynomial and the number of cells of the mesh, is used in the error estimates for such conservative scheme. Meanwhile the local L^2 projection is enough for the dissipative scheme which has no extra restrict on the approximation spaces and meshes. To the best of our knowledge, there is no study on the error estimates for the DG method to the DP equation because of the obstacles caused by the nonlinear term $4uu_x$ in (1.9). However, the term $3\mu(u)u_x$ of the μDP equation,

which is a linear term in some conservative sense, make us avoid this difficulty appeared in the DP equation. In this paper, we present two a priori error estimates for both conservative and dissipative schemes to the μDP equation and finally obtain two different results.

The LDG method discussed in present paper is an extension of the discontinuous Galerkin (DG) method to solve PDEs containing higher than first order spatial derivatives, using discontinuous piecewise polynomials as numerical solutions and test functions in the spacial variables. The LDG method was firstly constructed by Cockburn and Shu [7] in solving nonlinear convection-diffusion equations, which was inspired by the efficient numerical experiments of Bassi and Rebay [1] for simulating the compressible Navier-Stokes equations. In the procedure of the LDG method, higher order derivatives are rewritten into a first order system and applied with DG method subsequently. The cardinal technique in the LDG method is the design of the so-called numerical fluxes. The literatures on designing and analyzing the LDG schemes for different kinds of equations are quite plenty, and we suggest the reader consulting [7,18,20–23,25] and the references therein. These contributions about the LDG method could supply rich and efficient guidance for us when encountering new equations or similar problems.

The extremely local, element based discretization in the DG method is effectively favorable for parallel computing and retaining high-precision on unstructured meshes. Particularly, DG methods are well suited for hp-adaptation, which consists of local mesh refinement and the adjustment of the polynomial order in individual elements. The LDG schemes for the μCH (1.1) and μDP (1.11) equations in present paper keep all these good properties.

Our paper is organized as follows: In Sect. 2, notations and other preliminary materials, such as the function spaces are firstly introduced. Section 3 is devoted to the study of the LDG schemes for the μCH equation. In Sects. 3.2 and 3.3 , the conservation of E_0 and E_1 of the μCH equation are proved valid for the conservative scheme and the H_μ^1 error estimate of the scheme is also given. Besides, we also supplement a dissipative scheme for the μCH equation by altering the numerical fluxes and prove the corresponding stability according to E_1 and the error estimate. Section 4 is on the subject of the μDP equation. Similarly we design two LDG schemes for the μDP equation, one is conservative and the other one is dissipative. The evolution of Hamiltonian invariants H_0 and H_1 of the μDP equation is analyzed in Sect. 4.2. Then in Sect. 4.3, we give the L^2 error estimates of these two schemes. In Sect. 5, we implement these numerical schemes for some examples to illustrate the accuracy and capability of LDG schemes for both μCH and μDP equations. In particular, the features of admitting peakon solutions (for both μCH and μDP) and shock solutions (for μDP only) are numerically validated in this part. Concluding remarks are given in Sect. 6. Some proofs of several lemmas for the μCH equation are placed in "Appendix A".

2 Notations, Function Spaces and Norms

In the following discussion, we just take one period, denoted by $I = [0, L]$, of the whole domain $\mathbb{R}$ to replace the unit circle $\mathbb{S}$ by setting $L = 1$. Let $\mathcal{T}_h$ denote the partition of I with the mesh denoted by $I_j = [x_{j-\frac{1}{2}}, x_{j+\frac{1}{2}}]$ for $j = 1, \ldots, N$. The center of the cell is $x_j = \frac{1}{2}(x_{j-\frac{1}{2}} + x_{j+\frac{1}{2}})$ and the mesh size is denoted by $h_j = x_{j+\frac{1}{2}} - x_{j-\frac{1}{2}}$ with $h = \max_{1 \leq j \leq N} h_j$ being the maximum cell size. The mesh is assumed to be regular, which means the ratio between the maximum and minimum mesh sizes keeps bounded in the mesh refinements.

The so-called broken Sobolev spaces $W^{s,p}(\mathcal{T}_h)$ are the finite Cartesian products of the standard Sobolev spaces $W^{s,p}(I_j)$ on all cells in $\mathcal{T}_h$. Norms of $W^{s,p}(\mathcal{T}_h)$ with $p = 2, \infty$ are given by

$$\|u\|_{W^{s,2}(\mathcal{T}_h)} = \|u\|_{H^s(\mathcal{T}_h)} = \left(\sum_{j=1}^{N} \|u\|_{H^s(I_j)}^2 \right)^{\frac{1}{2}}, \quad \|u\|_{W^{s,\infty}(\mathcal{T}_h)} = \max_{1 \le j \le N} \|u\|_{W^{s,\infty}(I_j)}.$$

In the case $s = 0$ with the interval I being clear from context, we would like to use the norms $\|u\|$ and $\|u\|_\infty$ to connote $\|u\|_{L^2(\mathcal{T}_h)}$ and $\|u\|_{L^\infty(\mathcal{T}_h)}$, respectively. Then we choose the following discontinuous piecewise polynomial space as the finite element space

$$V_h = \left\{ v(x) : v(x) \in P^k(I_j), \text{ for } x \in I_j, \ j = 1, \dots, N \right\}, \tag{2.1}$$

where $P^k(I_j)$ denotes the set of polynomials of the degree up to k in each cell I_j. It transpires that the functions belonging to V_h could be discontinuous on the element interfaces.

The solution of the numerical scheme is denoted by u_h, which belongs to the finite element space V_h. We denote the values of u_h at $x_{j+\frac{1}{2}}$ by $(u_h)_{j+\frac{1}{2}}^+$ and $(u_h)_{j+\frac{1}{2}}^-$, from the right cell I_{j+1} and the left cell I_j, respectively. We use the usual notations $[u_h] = u_h^+ - u_h^-$ and $\{u_h\} = \frac{1}{2}(u_h^+ + u_h^-)$ to denote the jump and the mean of the function u_h, respectively, at each element boundary point.

3 The μ-Camassa–Holm Equation

In this section, we devote to construct and analyze a conservative LDG scheme for the μCH equation, verify the properties of preserving Hamiltonian invariants and give the detailed error estimates. Besides, a dissipative scheme for this equation is also presented and the Hamiltonian stability is given. The main structure of this part is guided by the study for the LDG method to the CH equation in [20].

3.1 The LDG Schemes for the μCH Equation

In this part, we apply the LDG method to the μCH equation (1.1) which is written in following equivalent form

$$\mu(u) - u_{xx} = q, \tag{3.1}$$

$$q_t + f(u)_x = \frac{1}{2}(u^2)_{xxx} - \frac{1}{2}\left((u_x)^2\right)_x, \tag{3.2}$$

with the initial condition

$$u(x, 0) = u_0(x), \tag{3.3}$$

and periodic boundary conditions

$$u(x, t) = u(x + L, t), \tag{3.4}$$

where L is the measure of one period in the x direction and $f(u) = 2\mu(u)u$.

To define the local discontinuous Galerkin method, we further rewrite (3.1) as a first-order system

$$\begin{cases} \mu(u) - r_x = q, \\ r - u_x = 0. \end{cases} \tag{3.5}$$

Assume that q is known and u is to be solved, then we can formulate the LDG method for (3.5) as follows: Find $u_h, r_h \in V_h$ such that, for all test functions $\chi, \phi \in V_h$,

$$\mu(u_h) \int_{I_j} \chi \, dx + \int_{I_j} r_h \chi_x \, dx - \left(\widehat{r_h} \chi^- \right)_{j+\frac{1}{2}} + \left(\widehat{r_h} \chi^+ \right)_{j-\frac{1}{2}} = \int_{I_j} q_h \chi \, dx, \qquad (3.6)$$

$$\int_{I_j} r_h \phi \, dx + \int_{I_j} u_h \phi_x - \left(\widehat{u_h} \phi^- \right)_{j+\frac{1}{2}} + \left(\widehat{u_h} \phi^+ \right)_{j-\frac{1}{2}} = 0. \qquad (3.7)$$

The "hat" terms in (3.6)–(3.7) appeared in the cell boundary terms are the so-called "numerical fluxes", which are single-valued functions defined on the nodes and should be designed to ensure the stability of the numerical schemes. For Eq. (3.5), we take the alternating fluxes such that

$$\widehat{r_h} = r_h^-, \quad \widehat{u_h} = u_h^+. \qquad (3.8)$$

For (3.2), we can also rewrite it into a first-order system

$$\begin{cases} q_t + f(u)_x - p_x + B(r)_x & = 0, \\ p - (b(r)u)_x & = 0, \\ r - u_x & = 0. \end{cases} \qquad (3.9)$$

where $B(r) = \frac{1}{2} r^2$ and $b(r) = B'(r) = r$. Now the LDG method for this system can be formulated as: Find $q_h, p_h, r_h \in V_h$ such that, for all test functions $\eta, \psi, \zeta \in V_h$,

$$\int_{I_j} (q_h)_t \eta \, dx - \int_{I_j} (f(u_h) - p_h + B(r_h)) \eta_x \, dx$$
$$+ \left(\left(\widehat{f} - \widehat{p_h} + \widehat{B(r_h)} \right) \eta^- \right)_{j+\frac{1}{2}} - \left(\left(\widehat{f} - \widehat{p_h} + \widehat{B(r_h)} \right) \eta^+ \right)_{j-\frac{1}{2}} = 0, \qquad (3.10)$$

$$\int_{I_j} p_h \psi \, dx + \int_{I_j} b(r_h) u_h \psi_x \, dx - \left(\widehat{b(r_h)} \widetilde{u}_h \psi^- \right)_{j+\frac{1}{2}} + \left(\widehat{b(r_h)} \widetilde{u}_h \psi^+ \right)_{j-\frac{1}{2}} = 0, \quad (3.11)$$

$$\int_{I_j} r_h \zeta \, dx + \int_{I_j} u_h \zeta_x \, dx - \left(\breve{u}_h \zeta^- \right)_{j+\frac{1}{2}} + \left(\breve{u}_h \zeta^+ \right)_{j-\frac{1}{2}} = 0. \qquad (3.12)$$

We choose the numerical fluxes in (3.10)–(3.12) as follows

$$\widehat{p_h} = p_h^-, \; \breve{u}_h = u_h^+, \; \widehat{B(r_h)} = B(r_h^-), \; \widehat{b(r_h)} = \frac{B(r_h^+) - B(r_h^-)}{r_h^+ - r_h^-}, \; \widetilde{u}_h = u_h^+, \qquad (3.13)$$

and the numerical flux $\widehat{f}(u_h^-, u_h^+)$ is Lipschitz continuous in both arguments and consistent ($\widehat{f}(u, u) = f(u)$). Choices of the monotone numerical fluxes $\widehat{f}$, which is non-decreasing in the first argument and non-increasing in the second argument, in DG methods for conservation laws can be found in [6]. In our paper, two different schemes are presented by the numerical flux $\widehat{f}$ being chosen as the following two scenarios.

- For a conservative scheme, we choose

$$\widehat{f}(u_h^-, u_h^+) = \frac{1}{2} \left(f(u_h^-) + f(u_h^+) \right). \qquad (3.14)$$

Since $\mu(u)$ is conserved, we can simplify the numerical flux as $\widehat{f}(u_h^-, u_h^+) = 2\mu_0\{u_h\}$, where $\mu_0 = \mu(u)$.

- For a dissipative scheme, the monotone numerical flux $\widehat{f}$ is chosen as the Lax-Friedrichs flux

$$\widehat{f}(u_h^-, u_h^+) = \frac{1}{2}(f(u_h^-) + f(u_h^+) - \alpha(u_h^+ - u_h^-)), \quad \alpha = \max_{u_h} |f'(u_h)|. \quad (3.15)$$

  For simplification, $\widehat{f}(u_h^-, u_h^+)$ can be chosen as the upwind flux based on the constant $\mu_0 = \mu(u)$.

Remark 3.1 We remark that the choices of the fluxes in (3.8) and (3.13) are not unique. The cardinal rule of choosing is that we must take the fluxes from opposite sides for each of the following couples: $\widehat{r}_h$ and $\widehat{u}_h$, $\widehat{p}_h$ and $\breve{u}_h$, $\widehat{B(r_h)}$ and $\widetilde{u}_h$. Here we list a sequence of possible choices of the numerical fluxes (using $\widehat{m}$ and $\widehat{n}$ as the representation notations): for all $j = 1, \ldots, N$

$$\widehat{m}_{j+\frac{1}{2}} = \{m\}_{j+\frac{1}{2}} + \theta([m])_{j+\frac{1}{2}},$$
$$\widehat{n}_{j+\frac{1}{2}} = \{n\}_{j+\frac{1}{2}} - \theta([n])_{j+\frac{1}{2}},$$

where θ is a constant. Particularly, θ taking $\pm\frac{1}{2}$ leads to the alternating fluxes and $\theta = 0$ to the central fluxes.

3.1.1 Algorithm Flowchart (I)

This section shows some details about the implementation of the numerical method.

- From (3.6)–(3.7) with the fluxes (3.8), we can obtain the relationships among $\mathbf{u}_h$, $\mathbf{r}_h$ and $\mathbf{q}_h$ in the matrix form

$$\mathbf{A}_\mu \mathbf{u}_h + \mathbf{B}_r \mathbf{r}_h = \mathbf{A} \mathbf{q}_h, \quad (3.16)$$
$$\mathbf{A}\mathbf{r}_h + \mathbf{B}_u \mathbf{u}_h = \mathbf{0}. \quad (3.17)$$

  where $\mathbf{r}_h$, $\mathbf{q}_h$ and $\mathbf{u}_h$ are the vectors containing the degrees of freedom for r_h, q_h and u_h, respectively. And the matrices $\mathbf{A}_\mu$, $\mathbf{B}_r$, $\mathbf{A}$ and $\mathbf{B}_u$ are the corresponding discrete operators in the scheme (3.6)–(3.7). We can deduce that

$$\mathbf{D}\mathbf{u}_h = \mathbf{A}\mathbf{q}_h, \quad (3.18)$$

  where $\mathbf{D} = \mathbf{A}_\mu - \mathbf{B}_r \mathbf{A}^{-1} \mathbf{B}_u$.
- Then from (3.10)–(3.12) equipped with the corresponding fluxes (3.13) and (3.14), we get the LDG discretization of the residue $-f(u)_x + \frac{1}{2}(u^2)_{xxx} - \frac{1}{2}((u_x)^2)_x$ as follows

$$\mathbf{A}(\mathbf{q}_h)_t = \mathbf{res}(\mathbf{u}_h). \quad (3.19)$$

- Combining (3.18) and (3.19), we get

$$\mathbf{D}(\mathbf{u}_h)_t = \mathbf{res}(\mathbf{u}_h). \quad (3.20)$$

- Finally, we can utilize a time discretization method to solve

$$(\mathbf{u}_h)_t = \mathbf{D}^{-1}\mathbf{res}(\mathbf{u}_h). \quad (3.21)$$

3.2 Hamiltonian Stability and Conservative Properties

In this part, we turn to establish the conservation of two invariants E_0 and E_1 of our numerical schemes designed for the μCH equation. Recall the definitions of E_0 and E_1

$$E_0(u) = \int_0^1 u\,dx, \qquad E_1(u) = \mu(u)^2 + \int_0^1 u_x^2\,dx.$$

Here we replace the unit circle $\mathcal{S}^1$ by the interval $[0, 1]$ in $\mathbb{R}$. We further define the discrete analogs to these two invariants of the LDG schemes

$$E_0^h(u_h) = \int_0^1 u_h\,dx, \qquad E_1^h(u_h) = \mu(u_h)^2 + \int_0^1 r_h^2\,dx. \tag{3.22}$$

Proposition 3.2 *Let u_h be the solution of the scheme* (3.6)–(3.7) *and* (3.10)–(3.12) *equipped with numerical fluxes* (3.8), (3.13) *in addition to* (3.14) *or* (3.15)*. Then the discrete versions of Hamiltonian invariants E_0^h and E_1^h satisfy*

- *The conservative scheme with numerical flux* (3.14) *for the μCH equation preserves the invariants E_0^h and E_1^h*

$$\frac{d}{dt}\big(\mu(u_h)\big) = 0, \quad \frac{d}{dt}\Big(\mu(u_h)^2 + \int_0^1 r_h^2\,dx\Big) = 0. \tag{3.23}$$

- *The dissipative scheme with numerical flux* (3.15) *for the μCH equation preserves only the invariant E_0^h yet keeps E_1^h stability*

$$\frac{d}{dt}\big(\mu(u_h)\big) = 0, \quad \frac{d}{dt}\Big(\mu(u_h)^2 + \int_0^1 r_h^2\,dx\Big) \leq 0. \tag{3.24}$$

Proof First, we consider the properties of E_0^h for both schemes. For (3.6), we first take the time derivative and obtain

$$\mu(u_h)_t \int_{I_j} \chi\,dx + \int_{I_j} (r_h)_t \chi_x\,dx - \big((\widehat{r}_h)_t \chi^-\big)_{j+\frac{1}{2}} + \big((\widehat{r}_h)_t \chi^+\big)_{j-\frac{1}{2}} = \int_{I_j} (q_h)_t \chi\,dx. \tag{3.25}$$

Since (3.25), (3.7) and (3.10)–(3.12) hold for any test functions in V_h, then by choosing

$$\chi = 1, \ \eta = 1, \ \phi = 0, \ \psi = 0, \ \zeta = 0,$$

we can get two valid equations

$$\mu(u_h)_t |I_j| - ((\widehat{r}_h)_t)_{j+\frac{1}{2}} + ((\widehat{r}_h)_t)_{j-\frac{1}{2}} = \int_{I_j} (q_h)_t\,dx,$$

$$\int_{I_j} (q_h)_t\,dx - \Big(\widehat{f} - \widehat{p_h} + \widehat{B(r_h)}\Big)_{j+\frac{1}{2}} + \Big(\widehat{f} - \widehat{p_h} + \widehat{B(r_h)}\Big)_{j-\frac{1}{2}} = 0,$$

where $|I_j| = \int_{I_j} 1\,dx$. Considering the periodic boundary condition, and summing up both equations over all cells, we obtain the conservation of E_0^h for both schemes

$$\mu(u_h)_t = 0.$$

Next, we turn to the analysis about E_1^h. Take the test functions in (3.25), (3.7) and (3.10)–(3.12) as follows

$$\chi = u_h, \phi = (r_h)_t, \eta = u_h, \psi = -r_h, \zeta = p_h. \tag{3.26}$$

Summing up these equations (3.25), (3.7) and (3.10)–(3.12), we obtain

$$\mu(u_h)_t \int_{I_j} u_h dx + \int_{I_j} (r_h)_t r_h dx - \int_{I_j} f(u_h)(u_h)_x dx + \left(\widehat{f}u_h^-\right)_{j+\frac{1}{2}} - \left(\widehat{f}u_h^+\right)_{j-\frac{1}{2}}$$

$$+ \int_{I_j} (p_h u_h)_x dx - \left(\widehat{p}_h u_h^- + \check{u}_h p_h^-\right)_{j+\frac{1}{2}} + \left(\widehat{p}_h u_h^+ + \check{u}_h p_h^+\right)_{j-\frac{1}{2}}$$

$$- \int_{I_j} (B(r_h)u_h)_x dx + \left(\widehat{B(r_h)}u_h^- + \widehat{b(r_h)}\widetilde{u}_h r_h^-\right)_{j+\frac{1}{2}} - \left(\widehat{B(r_h)}u_h^+ + \widehat{b(r_h)}\widetilde{u}_h r_h^+\right)_{j-\frac{1}{2}}$$

$$+ \int_{I_j} (u_h (r_h)_t)_x dx - \left((\widehat{r}_h)_t u_h^- + \widehat{u}_h (r_h^-)_t\right)_{j+\frac{1}{2}} + \left((\widehat{r}_h)_t u_h^+ + \widehat{u}_h (r_h^+)_t\right)_{j-\frac{1}{2}} = 0.$$

Taking $F(u) = \int^u f(\tau) d\tau$, we have

$$\mu(u_h)_t \int_{I_j} u_h dx + \int_{I_j} (r_h)_t r_h dx + \Psi_{j+\frac{1}{2}} - \Psi_{j-\frac{1}{2}} + \Theta_{j-\frac{1}{2}} = 0, \tag{3.27}$$

where the function $\Psi_{j+\frac{1}{2}}$, which will disappear for the reason of periodic boundary condition when summing up over all cells, are given by

$$\Psi_{j+\frac{1}{2}} = \left(-F(u_h^-) + \widehat{f}u_h^- + p_h^- u_h^- - (\widehat{p}_h u_h^- + \check{u}_h p_h^-)\right.$$

$$\left. - B(r_h^-)u_h^- + \widehat{B(r_h)}u_h^- + \widehat{b(r_h)}\widetilde{u}_h r_h^- + (r_h^-)_t u_h^- - ((\widehat{r}_h)_t u_h^- + \widehat{u}_h (r_h^-)_t))\right)_{j+\frac{1}{2}},$$

and the extra term Θ is given by

$$\Theta_{j-\frac{1}{2}} = \left([F(u_h)] - \widehat{f}[u_h] - [p_h u_h] + \widehat{p}_h[u_h] + \check{u}_h[p_h]\right.$$

$$\left. + [B(r_h)u_h] - \widehat{b(r_h)}\widetilde{u}_h[r_h] - \widehat{B(r_h)}[u_h] - [(r_h)_t u_h] + (\widehat{r}_h)_t[u_h] + \widehat{u}_h[(r_h)_t]\right)_{j-\frac{1}{2}}.$$

On account of the choices of the numerical fluxes in (3.8) and (3.13) and applying some algebraic manipulation, we have

$$-[p_h u_h] + \widehat{p}_h[u_h] + \check{u}_h[p_h] = 0,$$
$$[B(r_h)u_h] - \widehat{b(r_h)}\widetilde{u}_h[r_h] - \widehat{B(r_h)}[u_h] = 0,$$
$$-[(r_h)_t u_h] + (\widehat{r}_h)_t[u_h] + \widehat{u}_h[(r_h)_t] = 0.$$

Now the extra term $\Theta_{j-\frac{1}{2}}$ becomes

$$\Theta_{j-\frac{1}{2}} = ([F(u_h)] - \widehat{f}[u_h]_{j-\frac{1}{2}}). \tag{3.28}$$

- **Conservative scheme**

We first consider the conservative scheme with the numerical flux $\widehat{f}(u_h^-, u_h^+) = \frac{1}{2}(f(u_h^-) + f(u_h^+))$. Noticing that $\mu(u_h)_t = 0$, namely $\mu(u_h)$ is a constant in time evolution denoted by μ_0, then $\widehat{f}(u_h^-, u_h^+) = 2\mu_0\{u_h\}$ and this leads to

$$\Theta_{j-\frac{1}{2}} = \left([F(u_h)] - \widehat{f}[u_h]\right)_{j-\frac{1}{2}} = \int_{u_h^-}^{u_h^+} (f(s) - \widehat{f}(u_h^-, u_h^+))ds$$

$$= \int_{u_h^-}^{u_h^+} 2\mu_0 s\, ds - \mu_0\left((u_h^+)^2 - (u_h^-)^2\right) = 0.$$

Summing up the equalities (3.27), and noticing $\sum_{j=1}^{N} \int_{I_j} u_h\, dx = \mu(u_h)$, then we obtain the desired result (3.23) for the conservative scheme.

- **Dissipative scheme**

Besides, the dissipative scheme with numerical flux $\widehat{f}$ chosen as (3.15) has the only difference in the term $\Theta_{j-\frac{1}{2}}$ comparing to the conservative scheme. By the monotonicity and consistency of the Lax-Friedrichs flux, we have

$$\Theta_{j-\frac{1}{2}} = \left([F(u_h)] - \widehat{f}(u_h^-, u_h^+)[u_h]\right)_{j-\frac{1}{2}}$$

$$= \int_{u_h^-}^{u_h^+} \left(\widehat{f}(s,s) - \widehat{f}(s, u_h^+) + \widehat{f}(s, u_h^+) - \widehat{f}(u_h^-, u_h^+)\right) \geq 0.$$

This alteration gives rise to some dissipative E_1^h property of this scheme

$$\frac{d}{dt}\left(\mu(u_h)^2 + \int_0^1 r_h^2 dx\right) \leq 0.$$

$\square$

Remark 3.3 On account of the conservation of E_0^h, the essence of the conservation of E_1^h is

$$E_1^h = \int_0^1 r_h^2 dx, \qquad (3.29)$$

which indicates the L^2 energy of the numerical approximation to u_x.

Remark 3.4 There is another equivalent form of the CH or μCH equation

$$m_t + um_x + 2mu_x = 0, \qquad (3.30)$$

where $m = u - u_{xx}$ (for the CH equation) or $m = \mu(u) - u_{xx}$ (for the μCH equation). Based on this form, Liu and Xing present a fully-discrete invariant preserving DG method for the CH equation in [12]. The semi-discretization of their method can preserve the invariants spatially by choosing the central fluxes. We remark that this semi-discrete scheme can also be adapted to the μCH equation via almost the same procedures given in [12] except the last step of solving u from m. In the implementation of the scheme for the μCH equation, if we choose the central fluxes, the matrix $\mathbf{D} = \mathbf{A}_\mu - \mathbf{B}_r \mathbf{A}^{-1}\mathbf{B}_u$ in (3.18), which is generated by the operator $A = \mu - \partial_x^2$, will be singular without some essential restricts on the degree of polynomial of V_h and the number of cells in $\mathcal{T}_h$. This phenomenon also appears in the numerical experiments for the conservative LDG scheme for the μDP equation in next section, and therein we will give some detailed information about it.

3.3 Error Estimates of the LDG Method

In this subsection, we show the procedure to get the error estimates of our conservative and dissipative LDG schemes for the μCH equation.

3.3.1 Notations and Auxiliary Results

In this part, we introduce some notations and assumptions to be used and some auxiliary results to be cited later in this paper. We would define some projections and present certain interpolation and inverse properties for the finite element spaces.

• *Notations and assumptions* We will denote by C a positive constant independent of h, which may depend on the solution of the μCH equation considered in this paper. Besides, the constant C may have a different value in each occurrence for the sake of facility. In this part, the exact solution of the problem to be considered is assumed to be sufficiently smooth equipped with the periodic boundary conditions. The time evolution about the problem is also bounded as $0 \le t \le T$ for a fixed T. Consequently, the exact solution is bounded too.

• *Projection and interpolation properties* In the following, we will introduce the standard L^2 projection of a function ω with $k+1$ order bounded derivatives into the finite element space V_h, denoted by $\mathcal{P}$; i.e., for each j,

$$\int_{I_j} (\mathcal{P}\omega(x) - \omega(x))v(x)dx = 0 \quad for \quad \forall v \in P^k(I_j), \tag{3.31}$$

and the special projection $\mathcal{P}^\pm$ into V_h, satisfying that: for each j and $\forall v \in P^{k-1}(I_j)$,

$$\int_{I_j} (\mathcal{P}^+\omega(x) - \omega(x))v(x)dx = 0, \quad and \quad \mathcal{P}^+\omega(x^+_{j-\frac{1}{2}}) = \omega(x_{j-\frac{1}{2}}), \tag{3.32}$$

$$\int_{I_j} (\mathcal{P}^-\omega(x) - \omega(x))v(x)dx = 0, \quad and \quad \mathcal{P}^-\omega(x^-_{j+\frac{1}{2}}) = \omega(x_{j+\frac{1}{2}}). \tag{3.33}$$

For both projections mentioned above, authors in [26] generalized the following results from [5] as follows

$$\|\omega^e\| + h\|\omega^e\|_\infty + h^{\frac{1}{2}}\|\omega^e\|_{\Gamma_h} \le Ch^{k+1}, \tag{3.34}$$

where $\omega^e = \mathcal{P}\omega - \omega$ or $\omega^e = \mathcal{P}^\pm\omega - \omega$. The positive constant C depends only on ω, namely it is independent of h. Γ_h denotes the set of boundary points of all cells I_j belonging to the mesh grid, and the norm $\|u\|_{\Gamma_h} = \sqrt{\frac{1}{N}\sum_{j=1}^N \|u\|^2_{L^2(\partial I_j)}}$.

• *Inverse properties* We show several inverse properties of space V_h which will be utilized in the following error estimates. For any $\omega_h \in V_h$, there exists a positive constant C independent of ω_h and h, such that

$$(i)\|\nabla\omega_h\| \le Ch^{-1}\|\omega_h\|, \quad (ii)\|\omega_h\|_{\Gamma_h} \le Ch^{-\frac{1}{2}}\|\omega_h\|, \quad (iii)\|\omega_h\|_\infty \le Ch^{-\frac{1}{2}}\|\omega_h\|. \tag{3.35}$$

3.3.2 The Main Error Estimates Result

In what follows, we give the main error estimates of the semi-discrete LDG numerical schemes for the μCH equation. Both conservative and dissipative schemes are considered here, and the same results are obtained.

Theorem 3.5 *Let u be the exact solution of the problem* (3.1)–(3.2), *which is smooth enough with bounded derivatives. Let u_h be the numerical solution of the conservative or dissipative semi-discrete LDG scheme* (3.6)–(3.8) *and* (3.10)–(3.13) *equipped with numerical fluxes* (3.8) *and* (3.13) *in addition to* (3.14) *or* (3.15), *and denote the corresponding numerical error by $e_r = r - r_h$, where $r = u_x$ is defined by* (3.5). *For a regular partition of $I = [0, 1]$,*

we assume the finite element space V_h defined in (2.1) with kth-order piecewise polynomial, then for sufficiently small h, the following error estimate holds for both schemes

$$\|r - r_h\|^2 \leq Ch^{2k}, \tag{3.36}$$

where the constant C depends on the terminal time T, k, $\|u\|_{k+1}$, $\|r\|_{k+1}$, and the bound of $|f'|$. Here $\|u\|_{k+1}$ and $\|r\|_{k+1}$ are the maximum over $0 \leq t \leq T$ of the standard Sobolev $(k+1)$ norm in space.

Remark 3.6 In the Example 5.1 of Sect. 5, we see that the kth-order accuracy in (3.36) is optimal for $k \geq 1$. Moreover, recall the definition of the Hamiltonian energy $E_1(u)$ in (1.8) and the conservation of $\mu(u)$ and $\mu(u_h)$, then we recognize that the error estimate presented above is exactly the error equipped with the H_μ^1-norm. Although we could not get the error estimate for $u - u_h$, the numerical results in Example 5.1 verify the optimal convergence rate $\mathcal{O}(h^{k+1})$ for $\|u - u_h\|$.

- *The error equation* Now we need to put forward the proof of Theorem 3.5. It is necessary to obtain the error equation first.

Replacing u_h by the exact solution u in the scheme (3.6)–(3.7) and (3.10)–(3.12), the equations can also hold. Recalling the facts that $\mu(u)_t = 0$ and $\mu(u_h)_t = 0$, then it is easy to get the error equation: for any test functions $\chi, \phi, \eta, \psi, \zeta \in V_h$,

$$\int_{I_j} ((q - q_h)_t(\chi + \eta) + (r - r_h)\phi + (p - p_h)\psi + (r - r_h)\zeta) \, dx$$

$$- \int_{I_j} (r - r_h)_t \chi_x \, dx + \left((r_t - (\widehat{r_h})_t)\chi^-\right)_{j+\frac{1}{2}} - \left((r_t - (\widehat{r_h})_t)\chi^+\right)_{j-\frac{1}{2}}$$

$$+ \int_{I_j} (u - u_h)\phi_x \, dx - \left((u - \widehat{u_h})\phi^-\right)_{j+\frac{1}{2}} + \left((u - \widehat{u_h})\phi^+\right)_{j-\frac{1}{2}}$$

$$+ \int_{I_j} (p - p_h)\eta_x \, dx - \left((p - \widehat{p_h})\eta^-\right)_{j+\frac{1}{2}} + \left((p - \widehat{p_h})\eta^+\right)_{j-\frac{1}{2}}$$

$$+ \int_{I_j} (u - u_h)\zeta_x \, dx - \left((u - \breve{u}_h)\zeta^-\right)_{j+\frac{1}{2}} + \left((u - \breve{u}_h)\zeta^+\right)_{j-\frac{1}{2}}$$

$$- \int_{I_j} (B(r) - B(r_h))\eta_x \, dx + \left(\left(B(r) - \widehat{B(r_h)}\right)\eta^-\right)_{j+\frac{1}{2}} - \left(\left(B(r) - \widehat{B(r_h)}\right)\eta^+\right)_{j-\frac{1}{2}}$$

$$+ \int_{I_j} (b(r)u - b(r_h)u_h)\psi_x \, dx - \left(\left(b(r)u - \widehat{b(r_h)\widetilde{u}_h}\right)\psi^-\right)_{j+\frac{1}{2}}$$

$$+ \left(\left(b(r)u - \widehat{b(r_h)\widetilde{u}_h}\right)\psi^+\right)_{j-\frac{1}{2}}$$

$$- \int_{I_j} (f(u) - f(u_h))\eta_x \, dx + \left((f(u) - \widehat{f})\eta^-\right)_{j+\frac{1}{2}} - \left((f(u) - \widehat{f})\eta^+\right)_{j-\frac{1}{2}} = 0.$$

Define

$$\mathcal{B}_j(u - u_h, q - q_h, p - p_h, r - r_h; \chi, \phi, \eta, \psi, \zeta)$$

$$= \int_{I_j} ((q - q_h)_t(\chi + \eta) + (r - r_h)\phi + (p - p_h)\psi + (r - r_h)\zeta) \, dx$$

$$- \int_{I_j} (r - r_h)_t \chi_x \, dx + \left((r_t - (\widehat{r_h})_t)\chi^-\right)_{j+\frac{1}{2}} - \left((r_t - (\widehat{r_h})_t)\chi^+\right)_{j-\frac{1}{2}}$$

$$+ \int_{I_j} (u - u_h)\phi_x dx - \left((u - \widehat{u}_h)\phi^-\right)_{j+\frac{1}{2}} + \left((u - \widehat{u}_h)\phi^+\right)_{j-\frac{1}{2}}$$

$$+ \int_{I_j} (p - p_h)\eta_x dx - \left((p - \widehat{p_h})\eta^-\right)_{j+\frac{1}{2}} + \left((p - \widehat{p_h})\eta^+\right)_{j-\frac{1}{2}}$$

$$+ \int_{I_j} (u - u_h)\zeta_x dx - \left((u - \widecheck{u}_h)\zeta^-\right)_{j+\frac{1}{2}} + \left((u - \widecheck{u}_h)\zeta^+\right)_{j-\frac{1}{2}}, \tag{3.37}$$

$$\mathcal{H}_j(f; u, u_h \eta) = \int_{I_j} (f(u) - f(u_h))\eta_x dx - \left((f(u) - \widehat{f})\eta^-\right)_{j+\frac{1}{2}} + \left((f(u) - \widehat{f})\eta^+\right)_{j-\frac{1}{2}}, \tag{3.38}$$

and

$$\mathcal{R}_j(b, B; r, u, r_h, u_h; \eta, \psi)$$

$$= \int_{I_j} (B(r) - B(r_h))\,\eta_x dx - \left(\left(B(r) - \widehat{B(r_h)}\right)\eta^-\right)_{j+\frac{1}{2}} + \left(\left(B(r) - \widehat{B(r_h)}\right)\eta^+\right)_{j-\frac{1}{2}}$$

$$- \int_{I_j} (b(r)u - b(r_h)u_h)\psi_x dx + \left(\left(b(r)u - \widehat{b(r_h)}\widetilde{u}_h\right)\psi^-\right)_{j+\frac{1}{2}}$$

$$- \left(\left(b(r)u - \widehat{b(r_h)}\widetilde{u}_h\right)\psi^+\right)_{j-\frac{1}{2}}. \tag{3.39}$$

Summing over j, the error equation becomes

$$\sum_{j=1}^N \mathcal{B}_j(u - u_h, q - q_h, p - p_h, r - r_h; \chi, \psi, \eta, \psi, \zeta)$$

$$= \sum_{j=1}^N \left(\mathcal{H}_j(f; u, u_h; \eta) + \mathcal{R}_j(b, B; r, u, r_h, u_h; \eta, \psi)\right), \tag{3.40}$$

for all $\chi, \phi, \eta, \psi, \zeta \in V_h$.

Denoting

$$s = \mathcal{P}^+ u - u_h, \quad s^e = \mathcal{P}^+ u - u, \tag{3.41}$$

$$\xi = \mathcal{P}q - q_h, \quad \xi^e = \mathcal{P}q - q, \tag{3.42}$$

$$v = \mathcal{P}p - p_h, \quad v^e = \mathcal{P}p - p, \tag{3.43}$$

$$\delta = \mathcal{P}r - r_h, \quad \delta^e = \mathcal{P}r - r, \tag{3.44}$$

and taking the test functions

$$\chi = -s, \ \phi = \delta_t, \ \eta = s, \ \psi = -\delta, \ \zeta = v,$$

we obtain the important energy equality

$$\sum_{j=1}^N \mathcal{B}_j(s - s^e, \xi - \xi^e, v - v^e, \delta - \delta^e; -s, \delta_t, s, -\delta, v)$$

$$= \sum_{j=1}^N \left(\mathcal{H}_j(f; u, u_h; s) + \mathcal{R}_j(b, B; r, u, r_h, u_h; s, -\delta)\right). \tag{3.45}$$

• *Proof of the main result.* In this part, we will follow the ideas of [20] to give the main proof of Theorem 3.5. We shall analyze each term of the error equation (3.45), and some proofs of following lemmas will be given in "Appendix A".

Firstly, under the condition that the mean of the exact solution, namely $\mu(u)$, is conservative and the property of L^2 projection, we can verify the fact that the mean $\mu(u_h)$ and $\mu(\mathcal{P}^+ u)$ are also conservative quantities. The proof of this lemma will be given in "Appendix A.2".

Lemma 3.7 *Under the assumption of conservation of $\mu(u)$, the mean of the numerical solution $\mu(u_h)$ and the L^2 projection $\mu(\mathcal{P}^+ u)$ are also conservative; In other words, the errors $s = \mathcal{P}^+ u - u_h$, $s^e = \mathcal{P}^+ u - u$ and $u - u_h$ satisfy*

$$\mu(s)_t \equiv 0, \quad \mu(s^e)_t \equiv 0, \quad \mu(u - u_h)_t \equiv 0. \tag{3.46}$$

As for the left-hand side of the energy equation (3.45), we give the following lemma, and the proof will be shown in "Appendix A.3".

Lemma 3.8 *Under the discussion in Lemma 3.7, the following equation holds*

$$\sum_{j=1}^{N} \mathcal{B}_j(s - s^e, \xi - \xi^e, v - v^e, \delta - \delta^e; -s, \delta_t, s, -\delta, v) = \int_0^1 \delta_t \delta \, dx - \sum_{j=1}^{N} \left((\widehat{v}^e + \widehat{\delta_t^e})[s] \right)_{j+\frac{1}{2}}. \tag{3.47}$$

We then rewrite the right-hand side of the energy equation (3.45) into the following forms

$$\sum_{j=1}^{N} \mathcal{H}_j(f; u, u_h; s) = \sum_{j=1}^{N} \int_{I_j} (f(u) - f(u_h)) s_x \, dx + \sum_{j=1}^{N} \left((f(u) - f(\{u_h\}))[s] \right)_{j+\frac{1}{2}}$$

$$+ \sum_{j=1}^{N} \left((f(\{u_h\}) - \widehat{f})[s] \right)_{j+\frac{1}{2}}, \tag{3.48}$$

$$\sum_{j=1}^{N} \mathcal{R}_j(b, B; r, u, r_h, u_h; s, -\delta) = \sum_{j=1}^{N} \int_{I_j} (B(r) - B(r_h)) s_x \, dx$$

$$+ \sum_{j=1}^{N} ((B(r) - B(r_h^-))[s])_{j+\frac{1}{2}}$$

$$+ \sum_{j=1}^{N} \int_{I_j} (b(r)u - b(r_h)u_h) \delta_x \, dx$$

$$+ \sum_{j=1}^{N} \left((b(r)u - \widehat{b(r_h)} u_h^+)[\delta] \right)_{j+\frac{1}{2}}, \tag{3.49}$$

where we apply the periodic boundary conditions and recall the average notation for u_h as $\{u_h\} = \frac{1}{2}(u_h^+ + u_h^-)$.

The difference between the conservative and dissipative scheme only exits in the choices of numerical flux $\widehat{f}$ which is reflected in the term $\mathcal{H}_j$, yet the same estimate results for $\mathcal{H}_j$ of both schemes are given in the following lemma. The proof will be given in "Appendix A.4".

Lemma 3.9 *Suppose that the interpolation property (3.34) is satisfied; then we obtain the estimates for (3.48) with the numerical flux $\widehat{f}$ chosen as (3.14) or (3.15)*

$$\sum_{j=1}^{N} \mathcal{H}_j(f; u, u_h; s) \leq C \|s\|^2 + C h^{2k}. \tag{3.50}$$

The estimates for $\mathcal{R}_j$ in (3.49) are given in the following lemma, and as for the proof of this lemma, we refer the reader to Lemma 4.6 in [20].

Lemma 3.10 *Suppose that the interpolation property* (3.34) *is satisfied, then we have the following estimates for* (3.49)

$$\left| \sum_{j=1}^{N} \mathcal{R}_j(b, B; r, u, r_h, u_h; s, -\delta) \right|$$

$$\leq \sum_{j=1}^{N} \left(|b'(r)u\{\delta^e\}[\delta]| + |b(r)(\delta^e)^-[s]| \right)_{j+\frac{1}{2}} + \frac{1}{2}\|s\|^2 + C\|\delta\|^2 + Ch^{2k+2}. \quad (3.51)$$

Now it is the time to present the final error estimates (3.36). Combining (3.40), (3.47), (3.50) and (3.51), we obtain

$$\int_0^1 \delta_t \delta dx \leq \sum_{j=1}^{N} \left((\widehat{v^e} + \widehat{\delta_t^e})[s] \right)_{j+\frac{1}{2}}$$

$$+ \sum_{j=1}^{N} \left(|b'(r)u\{\delta^e\}[\delta]| + |b(r)(\delta^e)^-[s]| \right)_{j+\frac{1}{2}} + C\|s\|^2 + Ch^{2k} + C\|\delta\|^2.$$

By Young's inequality and the interpolation property (3.34), we can obtain

$$\sum_{j=1}^{N} \left((\widehat{v^e} + \widehat{\delta_t^e})[s] \right)_{j+\frac{1}{2}} \leq Ch^{2k} + \|s\|^2,$$

$$\sum_{j=1}^{N} \left(|b'(r)u\{\delta^e\}[\delta]| + |b(r)(\delta^e)^-[s]| \right)_{j+\frac{1}{2}} \leq Ch^{2k} + \|\delta\|^2 + \|s\|^2,$$

then the inequality becomes

$$\int_0^1 \delta_t \delta dx \leq C \left(\|s\|^2 + \|\delta\|^2 \right) + Ch^{2k}. \quad (3.52)$$

Till now, we have deduced a preliminary form for the final error estimate. We need some auxiliary tools to deal with the inequality (3.52).

Firstly, we introduce the Poincaré-Friedrichs inequality for $W^{p,1}(\mathcal{T}_h)$ functions (here we take $p = 2$ for our finite element space V_h) from Chapter 10 of [3]

$$\|w\| \leq C \left(\left| \int_I w dx \right| + \|w_x\| + \left(h^{-1} \sum_{j=1}^{N} ([w])_{j+\frac{1}{2}}^2 \right)^{\frac{1}{2}} \right), \quad (3.53)$$

for any $w \in H^1(\mathcal{T}_h)$. Here the positive constant C depends only on $\mathcal{T}_h$. Noticing that $s \in V_h \subseteq H^1(\mathcal{T}_h)$, together with $\mu(s) = 0$ in Lemma 3.7, we obtain

$$\|s\| \leq C \left(\|s_x\| + \left(h^{-1} \sum_{j=1}^{N} ([s])_{j+\frac{1}{2}}^2 \right)^{\frac{1}{2}} \right). \quad (3.54)$$

Secondly, to deal with (3.54), we refer the reader to the conclusion (4.17) in [15], which says

$$\|s_x\| + \sqrt{c_0 h^{-1}} \left(\sum_{j=1}^{N} ([s])_{j+\frac{1}{2}}^2 \right)^{\frac{1}{2}} \leq C\|\delta\| + Ch^{k+1}, \tag{3.55}$$

where the c_0 is a positive constant from the inverse properties (3.35), and C is independent of h but maybe depends on c_0.

Combining (3.52), (3.54) and (3.55), then we can obtain the desirable inequality for both conservative and dissipative schemes

$$\frac{1}{2} \frac{d}{dt} \left(\int_0^1 \delta^2 dx \right) \leq C\|\delta\|^2 + Ch^{2k}. \tag{3.56}$$

Finally, Theorem 3.5 follows by implementing (3.56) with the Gronwall's inequality.

4 The μ-Degasperis–Procesi Equation

In this section, by using the notations and preliminary materials given in Sect. 2, we turn to construct and analyze the LDG schemes for the μDP equation (1.2). We shall design a general form of the LDG method for the μDP equation and introduce the conservative and dissipative schemes by choosing different numerical fluxes. The Hamiltonian stability, conservative properties and error estimates for both two schemes for the μDP equation are all given in following parts.

4.1 The LDG Schemes for the μDP Equation

Recall the rewritten form of the μDP equation in (1.11)

$$u_t + uu_x + 3\mu(u)(A_\mu^{-1}u)_x = 0, \tag{4.1}$$

where A_μ is invertible. By introducing the auxiliary variables q and v, we once again rewrite this form into the following first-order system

$$u_t + f(u)_x + 3\mu(u)q = 0, \tag{4.2}$$

$$q - v_x = 0, \tag{4.3}$$

$$\mu(v) - q_x = u, \tag{4.4}$$

with the initial and periodic boundary conditions

$$u(x, 0) = u_0(x), \tag{4.5}$$

$$u(x, t) = u(x + L, t), \tag{4.6}$$

where L is the length of one period and $f(u) = \frac{1}{2}u^2$. Now we present a general form of the LDG schemes of (4.2)–(4.4): Find $u_h \in V_h$, s.t. for all test functions γ, ϕ and ψ

$$\int_{I_j} (u_h)_t \gamma \, dx + 3\mu(u_h) \int_{I_j} q_h \gamma \, dx$$

$$- \int_{I_j} f(u_h) \gamma_x \, dx + \left(\widehat{f}(u_h) \gamma^- \right)_{j+\frac{1}{2}} - \left(\widehat{f}(u_h) \gamma^+ \right)_{j-\frac{1}{2}} = 0, \tag{4.7}$$

$$\int_{I_j} q_h \phi \, dx + \int_{I_j} v_h \phi_x \, dx - \left(\widehat{v}_h \phi^- \right)_{j+\frac{1}{2}} + \left(\widehat{v}_h \phi^+ \right)_{j-\frac{1}{2}} = 0, \tag{4.8}$$

$$\mu(v_h) \int_{I_j} \psi \, dx + \int_{I_j} q_h \psi_x \, dx - \left(\widehat{q}_h \psi^- \right)_{j+\frac{1}{2}} + \left(\widehat{q}_h \psi^+ \right)_{j-\frac{1}{2}} = \int_{I_j} u_h \psi \, dx. \tag{4.9}$$

Two different schemes are induced by the numerical fluxes in (4.7)–(4.9) which are chosen as the following two scenarios

- The conservative numerical scheme

$$\widehat{v}_h = \{v_h\}, \ \widehat{q}_h = \{q_h\}, \ \widehat{f} = \frac{1}{6} \left((u_h^+)^2 + u_h^+ u_h^- + (u_h^-)^2 \right), \tag{4.10}$$

- The dissipative numerical scheme

$$\widehat{v}_h = \{v_h\} - \beta[v_h], \ \widehat{q}_h = \{q_h\} + \beta[q_h], \ \widehat{f}(u_h)$$
$$= \frac{1}{2} \left(f(u_h^-) + f(u_h^-) - \alpha(u_h^+ - u_h^-) \right), \tag{4.11}$$

where $\alpha = \max\limits_{u_h} |f'(u_h)|$ and $\beta = \text{sign}(\mu(u_h))$.

Here the choice of $\widehat{f}$ in the conservative scheme stems from the work of [2] and the flux $\widehat{f}$ in the dissipative scheme is the Lax-Friedrichs flux aforementioned in (3.15).

Remark 4.1 We remark that the fluxes $\widehat{v}_h$ and $\widehat{q}_h$ in the dissipative scheme depends on the sign of $\mu(u_h)$. For example, when $\mu(u_h) > 0$, the numerical fluxes are actually the alternating fluxes $\widehat{v}_h = v_h^-$ and $\widehat{q}_h = q_h^+$. Furthermore, like the discussion in Remark 3.1, we can also choose $\widehat{v}_h$ and $\widehat{q}_h$ in a larger range as follows

$$\widehat{v}_h = \{v_h\} - \beta(\theta)[v_h], \ \widehat{q}_h = \{q_h\} + \beta(\theta)[q_h],$$

where $\beta(\theta) = \text{sign}(\mu(u_h))\theta$ and $\theta \geq 0$ is a parameter. To achieve a compact stencil as it was done in [27], we would like to use the numerical fluxes as in (4.11) with setting $\theta = 1$.

4.1.1 Algorithm Flowchart (II)

This section shows some details about implementation of these two numerical schemes. And the matrices $\mathbf{A}$ and $\mathbf{A}_\mu$ below have the same meanings as in Algorithm flowchart (I).

- By (4.8)–(4.9) and the fluxes $\widehat{v}_h$ and $\widehat{q}_h$ defined in (4.10), we can obtain the relationships in matrix sense

$$\mathbf{A}\mathbf{q}_h + \mathbf{B}_v \mathbf{v}_h = \mathbf{0}, \tag{4.12}$$

$$\mathbf{A}_\mu \mathbf{v}_h + \mathbf{B}_q \mathbf{q}_h = \mathbf{A}\mathbf{u}_h, \tag{4.13}$$

where $\mathbf{v}_h$, $\mathbf{q}_h$ and $\mathbf{u}_h$ are the vectors containing degrees of freedom for v_h, q_h and u_h, respectively. And we state that different choices of numerical fluxes, $\widehat{q}$ and $\widehat{v}$, result in different matrices, $\mathbf{B}_v$ and $\mathbf{B}_q$. Manipulate these two equalities then we can obtain $\mathbf{v}_h$, $\mathbf{q}_h$ as follows

$$\mathbf{v}_h = \mathbf{D}^{-1}\mathbf{A}\mathbf{u}_h, \tag{4.14}$$

$$\mathbf{q}_h = -\mathbf{A}^{-1}\mathbf{B}_v\mathbf{v}_h. \tag{4.15}$$

where $\mathbf{D} = \mathbf{A}_\mu - \mathbf{B}_q\mathbf{A}^{-1}\mathbf{B}_v$.

- Next, by the virtue of the equation (4.7) equipped with $\widehat{f}$ and necessary data of $\mathbf{q}_h$ which can be expressed by u_h deduced in last step, we can further get the LDG discretization of the residual $(-f(u)_x - 3\mu(u)q)$ as follow

$$\mathbf{A}(\mathbf{u}_h)_t = \mathbf{res}(\mathbf{u}_h). \tag{4.16}$$

- Finally, we apply a temporal discretization to solve

$$(\mathbf{u}_h)_t = \mathbf{A}^{-1}\mathbf{res}(\mathbf{u}_h). \tag{4.17}$$

Remark 4.2 We remark that the matrix $\mathbf{A}_\mu$ which is formed by term $\mu(u)$ in the μDP (or μCH) equation performs on solving linear system not as well as the mass matrix $\mathbf{A}$ generated in the DP (or CH) equation. The mass matrix $\mathbf{A}$ possesses some nice properties, such as good condition number and invertibility, which are beneficial for the coefficient matrix $\mathbf{D}$ while the singular matrix $\mathbf{A}_\mu$ only provides necessary degrees of freedom to determine the uniqueness of numerical solution u_h. This fact will cause some undesired phenomena when applying the central fluxes to $\widehat{v}_h$ or $\widehat{q}_h$. In detail, by choosing central fluxes, coefficient matrix $\mathbf{D}$ is nonsingular only under essential assumptions of the order of P^k polynomial being even and the number of cells being odd, and we will show this phenomenon in the numerical experiments in Sect. 5.

4.2 Hamiltonian Stability and Conservative Properties

In this part, we turn to study the performance of our schemes on the H_0 and H_1 invariants. Recall the definitions of the first two Hamiltonian invariants in (1.10)

$$H_0(u) = \int_0^1 u dx, \qquad H_1(u) = \int_0^1 u^2 dx, \tag{4.18}$$

here the unit circle $\mathcal{S}$ is replaced by the interval $[0, 1]$. In fact, these two quantities represent the mean and L^2-norm of the numerical solution in each period. The choices of flux $\widehat{f}$ in (4.10) and (4.11) can result in different conclusions about the conservation of the discrete versions of the Hamiltonian invariants.

Proposition 4.3 *Let u_h be the numerical solution to the LDG scheme (4.7)–(4.9) equipped with numerical fluxes in (4.10) or (4.11). Then the discrete versions of Hamiltonian invariants of u_h, $H_0(u_h)$ and $H_1(u_h)$, satisfy the following properties in the time evolution*

- *The conservative scheme with numerical fluxes (4.10) for the μDP equation preserves both invariants H_0 and H_1*

$$\frac{d}{dt}\mu(u_h) = 0, \quad \frac{d}{dt}\left(\int_0^1 u_h^2 dx\right) = 0. \tag{4.19}$$

- *The dissipative scheme with numerical fluxes (4.11) for the μDP equation preserve only H_0 but still keeps the L^2 stability*

$$\frac{d}{dt}\mu(u_h) = 0, \quad \frac{d}{dt}\left(\int_0^1 u_h^2 dx\right) \leq 0. \tag{4.20}$$

Proof Take the test functions in (4.7)–(4.9) as follows

$$\gamma = u_h, \quad \phi = 1, \quad \psi = 3\mu(u_h)q_h, \tag{4.21}$$

then we can obtain three equations

$$\int_{I_j} (u_h)_t u_h dx + 3\mu(u_h)\int_{I_j} q_h u_h dx - \int_{I_j} f(u_h)(u_h)_x dx + \left(\widehat{f}u_h^-\right)_{j+\frac{1}{2}} - \left(\widehat{f}u_h^+\right)_{j-\frac{1}{2}} = 0,$$

$$3\mu(u_h)\left(\mu(v_h)\int_{I_j} q_h dx + \int_{I_j} q_h(q_h)_x - \left(\widehat{q}_h q_h^-\right)_{j+\frac{1}{2}} + \left(\widehat{q}_h q_h^+\right)_{j-\frac{1}{2}} - \int_{I_j} u_h q_h dx\right) = 0,$$

$$\int_{I_j} q_h dx - \left(\widehat{v}_h\right)_{j+\frac{1}{2}} + \left(\widehat{v}_h\right)_{j-\frac{1}{2}} = 0.$$

By summing up all the cells I_j, we immediately get the truth: $\mu(q_h) = 0$. Then combining the first two equations above, we obtain a simplified equality

$$\frac{1}{2}\frac{d}{dt}\left(\int_I u_h^2 dx\right) + \sum_{j=1}^N \left([F(u_h)] - \widehat{f}(u_h)[u_h]\right)_{j-\frac{1}{2}} - \sum_{j=1}^N 3\mu(u_h)\left(\left[\frac{1}{2}q_h^2\right] - \widehat{q}_h[q_h]\right)_{j-\frac{1}{2}} = 0, \tag{4.22}$$

where $F(u) = \int^u f(\tau)d\tau$.

Next, based on the two choices of numerical fluxes in (4.10) and (4.11), we discuss the H_1 energy stability in following two cases.

- **Conservative scheme**

In fact, we can rewrite the form of $\widehat{f}$ in (4.10) with an essential expression

$$\widehat{f}(u_h) = \frac{1}{3}\left(\frac{1}{2}(u_h^+)^2 + \frac{1}{2}(u_h^+ u_h^-) + \frac{1}{2}(u_h^-)^2\right) = \frac{[F(u_h)]}{[u_h]}, \tag{4.23}$$

when the jump $[u_h] \neq 0$. Besides, notice the transformation: $[\frac{1}{2}q^2] = \{q\} \cdot [q]$, then we realize that the numerical fluxes in (4.10) induce the following equalities

$$[F(u_h)] - \widehat{f}(u_h)[u_h] = 0, \tag{4.24}$$

$$\mu(u_h)(\frac{1}{2}[q_h^2] - \widehat{q}_h[q_h]) = 0. \tag{4.25}$$

We can prove that the conservative scheme can preserve the L^2-norm of solution u_h by substitute (4.24) and (4.25) into (4.22)

$$\frac{1}{2}\frac{d}{dt}\left(\int_I u_h^2 dx\right) = 0. \tag{4.26}$$

- **Dissipative scheme**

If we choose the numerical flux $\widehat{f}$ as the Lax-Friedrichs flux and apply the alternative numerical fluxes as $\widehat{q}_h = \{q_h\} + \beta[q_h]$ with $\beta = \text{sign}(\mu(u_h))$, then we subsequently get two inequalities at each node

$$[F(u_h)] - \widehat{f}(u_h)[u_h] \geq 0, \tag{4.27}$$

$$\mu(u_h)\left(\frac{1}{2}[q_h^2] - \widehat{q}_h[q_h]\right) = -\frac{1}{2}|\mu(u_h)|[q_h]^2 \leq 0, \tag{4.28}$$

where the first inequality follows from the monotonicity and consistency of the Lax-Friedrichs flux

$$[F(u_h)] - \widehat{f}(u_h)[u_h] = \int_{u^-}^{u^+} \left(f(\tau; \tau) - \widehat{f}(u^-; u^+) \right) d\tau \geq 0.$$

Substituting the above inequalities (4.27) and (4.28) into (4.22), we finally obtain the L^2 stability of the dissipative scheme

$$\frac{1}{2} \frac{d}{dt} \left(\int_I u_h^2 dx \right) \leq 0. \tag{4.29}$$

Now, we complete the proof of the H_1 energy analysis for both two schemes.

As to the conservation of H_0, we just retake the test function $\gamma = 1$ in (4.7) and sum up over j along with the periodic boundary condition, then it is easy to get

$$\int_I (u_h)_t dx + 3\mu(u_h)\mu(q_h) = 0. \tag{4.30}$$

Substitute $\mu(q_h) = 0$ into the above equality, then the conclusion comes out

$$\frac{d}{dt} \mu(u_h) = 0. \tag{4.31}$$

This result adapts to both the conservative and dissipative schemes for the μDP equation. □

4.3 Error Estimates of the LDG Method

In this part, two different error estimates of the conservative and dissipative schemes for the μDP equation mentioned in previous part are given. The framework of these two proofs are so similar that we would like to complete the analysis of the conservative scheme first and give the essential supplements for the dissipative scheme subsequently.

4.3.1 Notations and Auxiliary Results

Other than the notations and tools mentioned in the previous Sect. 3.3.1, more special tools are useful in our following estimates of the conservative scheme. We list them here.
• *Global projection and interpolation property.* In consideration of the central flux $\widehat{p}_h = \{p_h\}$ in the energy conservative scheme, we need to introduce a global L^2 projection of ω with $k + 1$ continuous derivatives into the finite element space V_h, denoted by $\mathcal{P}^\star$; i.e.,

$$\int_{I_j} \mathcal{P}^\star w(x) v_h dx = \int_{I_j} w(x) v_h dx, \ \forall v_h \in P^{k-1}(I_j),$$
$$\{\mathcal{P}^\star w\} = \{w\}, \ at \ x_{j+\frac{1}{2}}, \ j = 1, 2, \ldots, N, \tag{4.32}$$

This special global projection mentioned above is described in [13], which states that the existence and optimal approximation property of this projection can be obtained under the assumptions on the polynomial degree k being even and the number of cells N of the partition $\mathcal{T}_h$ being odd. And the authors in [9] give the detailed description about the approximation property as follow

Lemma 4.4 *Assume that u is sufficiently smooth and periodic. Further assume that $k \geq 0$ is even and the number of cells N of the partition $\mathcal{T}_h$ is odd. Then, the projection operator*

$\mathcal{P}^{\star}$ *is well-defined and possesses the following approximation properties: for $s = 0, 1$ and $p = 2, \infty$, there holds*

$$\|u - \mathcal{P}^{\star}u\|_{W^{s,p}(I_j)} \leq Ch_j^{1-s} \left(\sum_{I_i \in \mathcal{T}_h^N} h_i^k \|u\|_{W^{s+1,\infty}(I_i)} + \sum_{I_i \in \mathcal{T}_h \backslash \mathcal{T}_h^N} h_i^{k+1} \|u\|_{W^{s+2,\infty}(I_i)} \right),$$

(4.33)

for a constant C independent of I_j, where $\mathcal{T}_h^N$ is the set of cells whose length differs from at least one of its immediate neighbors.

We remark that for an uniform mesh, the number of cells at least one of whose immediate neighbors have different lengths is zero and so the estimate (4.33) become optimal. And in our paper, we just use this ideal uniform mesh for projection $\mathcal{P}^{\star}$.

4.3.2 The Main Error Estimates Result

In what follows, we give the main error estimates of the semi-discrete LDG schemes for the μDP equation.

Theorem 4.5 *Let u be the exact solution of the μDP equation (4.1), which is smooth enough with bounded derivatives. Let u_h be the numerical solutions of the semi-discrete LDG schemes (4.7)–(4.9) equipped with the numerical fluxes (4.10) or (4.11), and denote the corresponding numerical errors by $e_u = u - u_h$. For a regular partition of $I = [0, 1]$ with N cells, we assume the finite element spaces V_h defined in (2.1) with kth-order piecewise polynomial where $k \geq 1$. For sufficiently small h and assuming that $\|u_h(0) - u(0)\| = \mathcal{O}(h^{k+1})$, the following two error estimates hold*

- *The numerical solution u_h of the dissipative LDG scheme (4.7)–(4.9) equipped with the numerical fluxes (4.11) satisfies*

$$\|u - u_h\|^2 \leq Ch^{2k+1},$$

(4.34)

- *Further assume that k is even, N is odd and the partitions $\mathcal{T}_h$ is uniform, then the numerical solution u_h of the conservative LDG scheme (4.7)–(4.9) along with (4.10) satisfies*

$$\|u - u_h\|^2 \leq Ch^{2k},$$

(4.35)

where the constant C depends on the terminal time T, k, $\mu(u)$ and $\|u\|_{k+1}$. Here $\|u\|_{k+1}$ is the maximum over $0 \leq t \leq T$ of the standard Sobolev $(k + 1)$ norm in space.

4.3.3 The Error Equation

In what follows, we just simply assume $\beta = \text{sign}(\mu(u_h)) = 1$ in (4.11), and this indicates that the numerical flux $\widehat{q}_h = q_h^+$ in the dissipative scheme. And the other case with $\mu(u_j) < 0$ can be easily proven following the analog strategy.

Recognize that the weak formulation (4.7)–(4.9) is also available when replacing u_h by u, then we can get the error equation

$$\int_{I_j} (u - u_h)_t \gamma \, dx + 3\mu_0 \int_{I_j} (q - q_h) \gamma \, dx - \int_{I_j} (u - u_h) \psi \, dx$$
$$+ \int_{I_j} (q - q_h) \psi_x \, dx - \left((q - \widehat{q}_h)\psi^-\right)_{j+\frac{1}{2}} + \left((q - \widehat{q}_h)\psi^+\right)_{j-\frac{1}{2}}$$
$$- \int_{I_j} (f(u) - f(u_h)) \gamma_x \, dx + \left((f(u) - \widehat{f}(u_h))\gamma^-\right)_{j+\frac{1}{2}} - \left((f(u) - \widehat{f}(u_h))\gamma^+\right)_{j-\frac{1}{2}} = 0,$$

here we use the constant $\mu_0 = \mu(u_h)$ on account of it being a conserved quantity. Then we divide the error equation into two parts

$$\mathcal{B}_j(u - u_h, q - q_h; \gamma, \psi) = \int_{I_j} (u - u_h)_t \gamma \, dx + 3\mu_0 \int_{I_j} (q - q_h) \gamma \, dx - \int_{I_j} (u - u_h) \psi \, dx$$
$$+ \int_{I_j} (q - q_h) \psi_x \, dx - \left((q - \widehat{q}_h)\psi^-\right)_{j+\frac{1}{2}} + \left((q - \widehat{q}_h)\psi^+\right)_{j-\frac{1}{2}},$$
$$(4.36)$$

and

$$\mathcal{H}_j(f; u, u_h; \gamma) = \int_{I_j} (f(u) - f(u_h)) \gamma_x \, dx - \left((f(u) - \widehat{f}(u_h))\gamma^-\right)_{j+\frac{1}{2}}$$
$$+ \left((f(u) - \widehat{f}(u_h))\gamma^+\right)_{j-\frac{1}{2}}.$$
$$(4.37)$$

Now we denote

$$s = \mathcal{P}u - u_h, \quad s^e = \mathcal{P}u - u, \quad (4.38)$$
$$\sigma = \widetilde{\mathcal{P}}q - q_h, \quad \sigma^e = \widetilde{\mathcal{P}}q - q, \quad (4.39)$$
$$\omega = \mathcal{P}v - v_h, \quad \omega^e = \mathcal{P}v - v, \quad (4.40)$$

here the new notation $\widetilde{\mathcal{P}}$ can be choose as $\mathcal{P}^\star$ and $\mathcal{P}^+$ for the conservative and dissipative schemes, respectively. Then the error equation becomes

$$\sum_{j=1}^{N} \mathcal{B}_j(s - s^e, \sigma - \sigma^e; \gamma, \psi) = \sum_{j=1}^{N} \mathcal{H}_j(f; u, u_h; \gamma). \quad (4.41)$$

Taking the test functions

$$\gamma = s, \quad \psi = 3\mu_0 \sigma, \quad (4.42)$$

we can get the important energy equality

$$\sum_{j=1}^{N} \left(\mathcal{B}_j(s, \sigma; s, \sigma) - \mathcal{B}_j(s^e, \sigma^e; s, \sigma)\right) = \sum_{j=1}^{N} \mathcal{H}_j(f; u, u_h; s). \quad (4.43)$$

4.3.4 Proof of the Main Result

In this part, we follow ideas of the proof for the μCH equation in previous section to analyze each term of the energy equation (4.43). And for the sake of textual coherence, we would like to keep our mind on the analysis of the conservative scheme, and supplement the residual proof for the dissipative-scheme subsequently.

- **Error estimates for the conservative scheme**

For the first term in the LHS of (4.43), we reuse the similar technology in the verification of the conservation laws in Proposition 4.3, to obtain

$$\sum_{j=1}^{N} \mathcal{B}_j(s, \sigma; s, \sigma) = \sum_{j=1}^{N} \int_{I_j} s_t s dx. \tag{4.44}$$

As to the second term of LHS in (4.43), we have

$$
\begin{aligned}
&\mathcal{B}_j(s^e, \sigma^e; s, \sigma) \\
&= \int_{I_j} s_t^e s dx + 3\mu_0 \int_{I_j} \sigma^e s dx - 3\mu_0 \int_{I_j} s^e \sigma dx + \int_{I_j} \sigma^e \sigma_x dx - \left(\widehat{\sigma}^e \sigma^-\right)_{j+\frac{1}{2}} + \left(\widehat{\sigma}^e \sigma^+\right)_{j-\frac{1}{2}} \\
&= \int_{I_j} s_t^e s dx - 3\mu_0 \int_{I_j} s^e \sigma dx + \int_{I_j} \sigma^e \sigma_x dx \\
&\quad + 3\mu_0 \int_{I_j} \sigma^e s dx + \left(\widehat{\sigma}^e [\sigma]\right)_{j+\frac{1}{2}} - \left(\widehat{\sigma}^e \sigma^+\right)_{j+\frac{1}{2}} + \left(\widehat{\sigma}^e \sigma^+\right)_{j-\frac{1}{2}}. \tag{4.45}
\end{aligned}
$$

Because $\mathcal{P}$ is a local L^2 projection and $\widetilde{\mathcal{P}} = \mathcal{P}^\star$ in (4.39) have the property that $\sigma^e = \mathcal{P}^\star q - q$ is locally orthogonal to all polynomials of degree up to $k - 1$, we have

$$\int_{I_j} s_t^e s dx - 3\mu_0 \int_{I_j} s^e \sigma dx + \int_{I_j} \sigma^e \sigma_x dx = 0.$$

By virtue of the special definition of $\{\mathcal{P}^\star q\} = \{q\}$ at the nodes and the flux $\widehat{\sigma}^e = \{\mathcal{P}^\star q\} - \{q\}$ in the conservative scheme, we also get

$$\left(\widehat{\sigma}^e [\sigma]\right)_{j+\frac{1}{2}} = 0. \tag{4.46}$$

Thus the equality (4.45) becomes

$$\mathcal{B}_j(s^e, \sigma^e; s, \sigma) = 3\mu_0 \int_{I_j} \sigma^e s dx - \left(\widehat{\sigma}^e \sigma^+\right)_{j+\frac{1}{2}} + \left(\widehat{\sigma}^e \sigma^+\right)_{j-\frac{1}{2}}.$$

Combine the above equation with (4.44), sum up over j, and take into consideration the periodic boundary condition, then we finally obtain

$$\sum_{j=1}^{N} \left(\mathcal{B}_j(s, \sigma; s, \sigma) - \mathcal{B}_j(s^e, \sigma^e; s, \sigma)\right) = \int_0^1 s_t s dx - 3\mu_0 \int_0^1 \sigma^e s dx. \tag{4.47}$$

To deal with the nonlinearity of the flux $f(u)$ in the RHS of (4.43), we make the a priori assumption first: for arbitrary $t^\star \in (0, T]$,

$$h^{-1} \|s(t)\|_{L^\infty(0,1)} + \|s_x(t)\|_{L^\infty(\mathcal{T}_h)} \leq 1, \quad \forall t \in [0, t^\star]. \tag{4.48}$$

Then we introduce the result of Proposition 3.3 in [2] under the a priori assumption mentioned above

$$\left| \sum_{j=1}^{N} \mathcal{H}_j(f; u, u_h; s) \right| \leq C \|s\|^2 + C h^k \|s\|. \tag{4.49}$$

We remark that the a priori assumption validates for $t \in [0, T]$ automatically when $k \geq 2$ and the initial condition satisfies $\|u_h(0) - u(0)\| = \mathcal{O}(h^{k+1})$ as $h \downarrow 0$ and the mesh size h

is sufficiently small with an upper boundary h_0 depending on u and T. We refer the reader to the detailed discussion about this conclusion in [2].

Combining (4.47) and (4.49), we can get

$$\int_0^1 s_t s\, dx \leq 3\mu_0 \int_0^1 \sigma^e s\, dx + C\|s\|^2 + Ch^k\|s\|. \tag{4.50}$$

We already know that μ_0 is a constant, thus we can get the following error estimates

$$\frac{1}{2}\frac{d}{dt}\int_0^1 s^2 dx \leq C\|s\|^2 + Ch^{2k}. \tag{4.51}$$

Finally, under assumptions on the polynomial degree k being even and the number of cells in an uniform mesh being odd, we get the desired error estimate

$$\|u - u_h\|^2 \leq Ch^{2k}. \tag{4.52}$$

Till now we complete the error analysis of the conservative scheme.

- **Error estimates for the dissipative scheme**

Now we turn to supplement the analogous analysis of the dissipative scheme for the μDP equation. Based on the structure of proof mentioned above, we alter the choice of numerical fluxes in scheme (4.7)–(4.9) by the dissipative ones (4.11) and replace the global L^2 projection $\mathcal{P}^\star$ in (4.39) by the local projection $\mathcal{P}^+$ defined in (3.32). Consequently these changes cause some essential modifications in the process of error analysis:

(i) The term $\mathcal{B}_j(s, \sigma; s, \sigma)$ estimated in (4.44) is no more a conservative one

$$\sum_{j=1}^N \mathcal{B}_j(s, \sigma; s, \sigma) \leq \int_0^1 s_t s\, dx,$$

and this fact can be easy obtained via the analogous analysis referring to (4.27), (4.28) and (4.29) in the proof of L^2 stability of the dissipative scheme.

(ii) The simultaneous alternation of fluxes and projection of in the dissipative scheme keeps the equality (4.46) still valid

$$\left(\widehat{\sigma}^e[\sigma]\right)_{j+\frac{1}{2}} = 0. \tag{4.53}$$

(iii) The choice of the Lax-Friedrichs flux $\widehat{f}$ will result in a different analysis about the term $\sum_{j=1}^N \mathcal{H}_j(f; u, u_h; s)$ in (4.43), yet Xu and Shu in [20] have already constructed the estimates for it

$$\sum_{j=1}^N \mathcal{H}_j(f; u, u_h; s)$$
$$\leq -\frac{1}{4}\alpha(\widehat{f}; u_h)[s]^2 + (C + C_\star(\|s\|_\infty + h^{-1}\|e_u\|_\infty^2))\|s\|^2$$
$$+ (C + C_\star h^{-1}\|e_u\|_\infty^2)h^{2k+1},$$

where $C_\star$ is a positive constant depending on the maximum of $|f''|$ and the non-negative function $\alpha(\widehat{f}; u_h)$ is the important quantity of measuring the difference between numerical flux $\widehat{f}$ and the physical flux f, which is in detail described in [26].

Combine these above modifications together and apply some manipulations, we get

$$
\int_0^1 s_t s \, dx + \frac{1}{4} \alpha(\widehat{f}; u_h)[s]^2
$$
$$
\leq 3\mu_0 \int_0^1 \sigma^e s \, dx + \left(C + C_\star \left(\|s\|_\infty + h^{-1} \|e_u\|_\infty^2 \right) \right) \|s\|^2 + \left(C + C_\star h^{-1} \|e_u\|_\infty^2 \right) h^{2k+1},
$$
$$
\leq \left(C + C_\star \left(\|s\|_\infty + h^{-1} \|e_u\|_\infty^2 \right) \right) \|s\|^2 + \left(C + C_\star h^{-1} \|e_u\|_\infty^2 \right) h^{2k+1} + C h^{2k+2}.
$$
(4.54)

Taking account of the positive property of $\alpha(\widehat{f}; u_h)$, the Young's inequality and the a priori assumption with $k \geq 1$, we can further get the following inequality

$$
\frac{1}{2} \frac{d}{dt} \int_0^1 s^2 \, dx \leq C(\|s\|^2) + C h^{2k+1}.
$$
(4.55)

Finally, we obtain the error estimate of this dissipative scheme for the μDP equation

$$
\|u - u_h\|^2 \leq C h^{2k+1}.
$$

Here assumptions about the parity of order of polynomial, number of cells and the uniform mesh can be omitted.

5 Numerical Results

In what follows, we give several numerical examples for each μ-version equation. Accuracy experiments for smooth travelling waves and simulations for peakon solutions are successively presented and validated for both μCH and μDP equations. Besides, the explicit total variation diminishing (TVD) Runge–Kutta method in [14], also known as strong stability preserving (SSP) Runge–Kutta method in [8], is utilized as the temporal discretization in following experiments. As we know, for the purpose of maintaining the conservative property of the fully discrete scheme, it is better to choose a conservative time discretization method, such as the midpoint method used in [2,12]. While the nonlinear terms in both two equations make it not very efficient in the performance of computing. Thus we choose the explicit Runge–Kutta methods, with the time step $\Delta t = 0.1 \Delta x$. The numerical scheme will be verified available in that the numerical results are convergent in a sequence of successive mesh refinement and the concerned conservation of invariants keeps numerically even in the peakon solutions.

In [11], a class of multi-peakons solutions for both μCH and μDP equations and a series of multi-shocks solutions for the μDP equation are given via explicit expressions. For the sake of facility and concision, we list here these expressions in advance.

Firstly, we introduce the multi-peakons waves for both equations. The exact solutions with M peaks take the form of

$$
u(x, t) = \sum_{i=1}^{M} p_i(t) g(x - q^i(t)),
$$
(5.1)

where $g(x)$ is the Green's function given by

$$
g(x) = \frac{1}{2} x(x - 1) + \frac{13}{12}, \quad \text{for } x \in [0, 1),
$$
(5.2)

and is extended periodically to $\mathbb{R}$, namely

$$g(x - x') = \frac{(x - x')^2}{2} - \frac{|x - x'|}{2} + \frac{13}{12}, \quad for \; x \in [x', x' + 1), \tag{5.3}$$

where x' denotes a translation of one periodic interval. The variables $p_i(t)$ and $q^i(t)$ depend on time t and they evolve according to

$$\dot{q}^i = \sum_{j=1}^{M} p_j g(q^i - q^j), \quad \dot{p}_i = -(\lambda - 1) \sum_{j=1}^{M} p_i p_j g'(q^i - q^j),$$

here λ is defined in (1.4) and the μCH and μDP are cases $\lambda = 2$ and $\lambda = 3$, respectively. And the value zero is assigned to the otherwise undetermined derivative $g'(x)$. In other words,

$$g'(x) := \begin{cases} 0, & x = 0, \\ x - \frac{1}{2}, & 0 < x < 1. \end{cases} \tag{5.4}$$

Secondly, we list the expressions of multi-shocks solutions for the μDP equation

$$u = \sum_{i=1}^{M} \left(p_i g(x - q^i) + s_i g'(x - q^i) \right). \tag{5.5}$$

The components in above equation evolve according to

$$\begin{aligned} \dot{q}^i &= u(q^i), \\ \dot{p}_i &= 2(s_i \{u_{xx}(q^i)\} - p_i \{u_x(q^i)\}), \\ \dot{s}_i &= -s_i \{u_x(q^i)\}, \end{aligned} \tag{5.6}$$

where

$$\{u_x(q^i)\} = \sum_{j=1}^{N} p_j g'(q^i - q^j) + \sum_{j=1}^{N} s_j, \quad \left\{u_{xx}(q^i)\right\} = \sum_{j=1}^{N} p_j,$$

and $g'(x)$ is defined by (5.4).

5.1 The μCH Equation

In this part, numerical experiments are designed to show the accuracy and capability of the conservative and dissipative schemes for the μCH equation

$$\mu(u)_t - u_{xxt} = -2\mu(u)u_x + 2u_x u_{xx} + u u_{xxx}. \tag{5.7}$$

As mentioned before, the difference between these two schemes for the μCH only exists in the choice of numerical flux for the term $f(u) = 2\mu(u)u$. In fact, this different choices cause very small influence on numerical results in that $f(u)$ with constant $\mu(u)$ is no more a nonlinear term. We will see this phenomenon in the numerical sense in following experiments.

Example 5.1 Smooth periodic waves for μCH

In [10], the authors present that the smooth travelling waves are of the form $u(x,t) = \phi(x - ct)$ where ϕ is a solution of the ODE

$$\phi_{xx} = \frac{2\mu_0(M - \phi)(\phi - m)}{c - \phi}. \tag{5.8}$$

The constant M, m and c in (5.8) can be set under the condition $m < c < M$ which brings about a smooth periodic traveling wave $\phi(x - ct)$ with $\min_{x \in \mathbb{R}} \phi(x) = m$ and $\max_{x \in \mathbb{R}} \phi(x) = M$. Here we choose $M = 1.5$, $m = 0.5$, and $c = 2$. It leads to a smooth periodic travelling wave with $period = 2.73321849515629$ and

$$\mu_0 = \mu(\phi) = \int_0^{period} \phi(x)dx = 2.55499933801271.$$

The ODE can be evolved from an initial condition for ϕ

$$\phi(0.796433828683979) = 1, \tag{5.9}$$

which can be computed by setting $\theta = \frac{\pi}{2}$ in (6.10) in [10]. Then we can get a high-precision numerical solution of (5.8) by utilizing the fourth-order Runge–Kutta method with 40,000 points. We apply the conservative and dissipative LDG schemes discussed in Sect. 3.1 to test this smooth solution of the μCH equation. The L^2 and H_μ^1 errors and orders of accuracy for both two schemes at time $t = 0.5$ are showed in Table 1. For the error computation in our paper, we just split each element into uniform 20 subintervals and compute the discrete L^2/H_μ^1 norm on these points. In the process of implementation, periodic boundary conditions and uniform meshes are used. The numerical results show that the numerical schemes with P^k elements give a $(k + 1)$th order of accuracy for u in the L^2-norm, and kth order in H_μ^1 norm. That is the fact that H_μ^1 norm of $u - u_h$ is equivalent to $\|r - r_h\|$ for the reason of $\mu(u - u_h) = 0$. This illustrates that our method is numerically optimal for u and r. Meanwhile, as we analyzed before, these two schemes have a really tiny difference from each other on account of the linearization of $f(u) = 2\mu(u)u$ with the operator μ, and the experiment here verifies this judgment: the numerical solutions for both schemes in Table 1 are close to each other in acceptable error ranges. For the conservative scheme, people usually expect accuracy reduction with odd order polynomials, but the optimal convergence rate has been found for our conservative scheme. This may be caused by the degeneration of the "nonlinear" term $f(u) = 2\mu(u)u_x$ to "linear" term for the conservation of $\mu(u)$. Also, it is found that the P^0 case achieves some superconvergence than expected.

Example 5.2 Periodic one-peakon solution for μCH

Referring to the explicit expression (5.1) of the peakon solution, we take one peak with $M = 1$, and set the initial data as

$$p_1(0) = 0.1, \ q^1(0) = 0.$$

For $x \in [0, 1]$ and the solution will be extended periodically to $\mathbb{R}$. We implement both the conservative scheme and the dissipative one to simulate the peakon solution of the μDP equation. The P^4 polynomial element, fourth order TVD Runge–Kutta method and a partition with $N = 160$ cells are used in the process of computation. The Fig. 1, containing the peak profiles at time $t = 0, 1, 5, 10, 15$ clearly shows us that these two schemes can simulate the periodic one-peakon solution well. The differences, $|E_0(t) - E_0(0)|$ and $|E_1(t) - E_1(0)|$,

Table 1 Example 5.1, accuracy test for the μCH equation (5.7) with exact smooth solution (5.8)

N	Dissipative scheme				Conservative scheme			
	L^2 Error	Order	H_μ^1 error	Order	L^2 error	Order	H_μ^1 error	Order
P^0								
10	1.8779e−01	–	7.4790e−01	–	9.8314e−02	–	6.9597e−01	–
20	9.4577e−02	0.9895	3.9228e−01	0.9310	2.8210e−02	1.8012	3.1496e−01	1.1438
40	4.7836e−02	0.9834	1.9349e−01	1.0196	7.4335e−03	1.9241	1.4070e−01	1.1625
80	2.4220e−02	0.9819	9.4650e−02	1.0316	1.8869e−03	1.9781	6.4903e−02	1.1163
160	1.2215e−02	0.9875	4.6652e−02	1.0207	4.7355e−04	1.9944	3.1011e−02	1.0655
P^1								
10	1.8965e−02	–	2.0286e−01	–	1.9663e−02	–	2.2355e−01	–
20	5.2058e−03	1.8652	1.0581e−01	0.9391	5.2815e−03	1.8964	1.1183e−01	0.9992
40	1.3249e−03	1.9743	5.3963e−02	0.9714	1.3340e−03	1.9852	5.5565e−02	1.0091
80	3.3264e−04	1.9938	2.7313e−02	0.9824	3.3379e−04	1.9988	2.7722e−02	1.0031
160	8.3212e−05	1.9991	1.3749e−02	0.9903	8.3356e−05	2.0016	1.3852e−02	1.0009
P^2								
10	3.0757e−03	–	4.8825e−02	–	3.1012e−03	–	5.0042e−02	–
20	2.9183e−04	3.3977	6.2321e−03	2.9698	2.9340e−04	3.4019	6.3079e−03	2.9879
40	3.0741e−05	3.2469	1.2048e−03	2.3709	3.0800e−05	3.2519	1.2111e−03	2.3808
80	3.5111e−06	3.1302	2.3230e−04	2.3747	3.5133e−06	3.1320	2.3282e−04	2.3791
160	4.0894e−07	3.1020	4.2573e−05	2.4480	4.0902e−07	3.1026	4.2611e−05	2.4499
P^3								
10	1.5357e−04	–	2.0634e−03	–	1.5395e−04	–	2.0885e−03	–
20	1.2239e−05	3.6493	3.3285e−04	2.6321	1.2274e−05	3.6488	3.3556e−04	2.6378
40	7.8730e−07	3.9584	5.3099e−05	2.6481	7.8887e−07	3.9597	5.3407e−05	2.6515
80	4.4310e−08	4.1512	7.2458e−06	2.8735	4.4397e−08	4.1512	7.2797e−06	2.8751
160	2.7785e−09	3.9953	9.0301e−07	3.0043	2.7817e−09	3.9964	9.0548e−07	3.0071

Uniform meshes with N cells at time $t = 0.5$

describing the evolution of two invariants are showed in the last graph in Fig. 1. It shows that $E_0(u_h)$ and $E_1(u_h)$ keep numerically conservative in both two schemes when simulating one-peakon solution for the μCH equation.

Example 5.3 Periodic three-peakons solution for μCH

In this example, we take $M = 3$ in (5.1) to study the case of three-peakons solution to the μCH equation (5.7) with the initial condition

$$u_0(x) = \sum_{i=1}^{3} p_i(0)g(x - q^i(0)), \tag{5.10}$$

where g, p_i and q^i, $i = 1, 2, 3$, are set as follows:

$$p_1(0) = 0.1, \ q^1(0) = 0.5, \ p_2(0) = 0.08, \ q^2(0) = 0.2, \ p_3(0) = 0.12, \ q^3(0) = 0.05.$$

The computational domain is [0, 1]. The P^4 polynomial elements with $N = 160$ cells is utilized in our numerical method. In Fig. 2, the numerical and exact solutions at $t =$
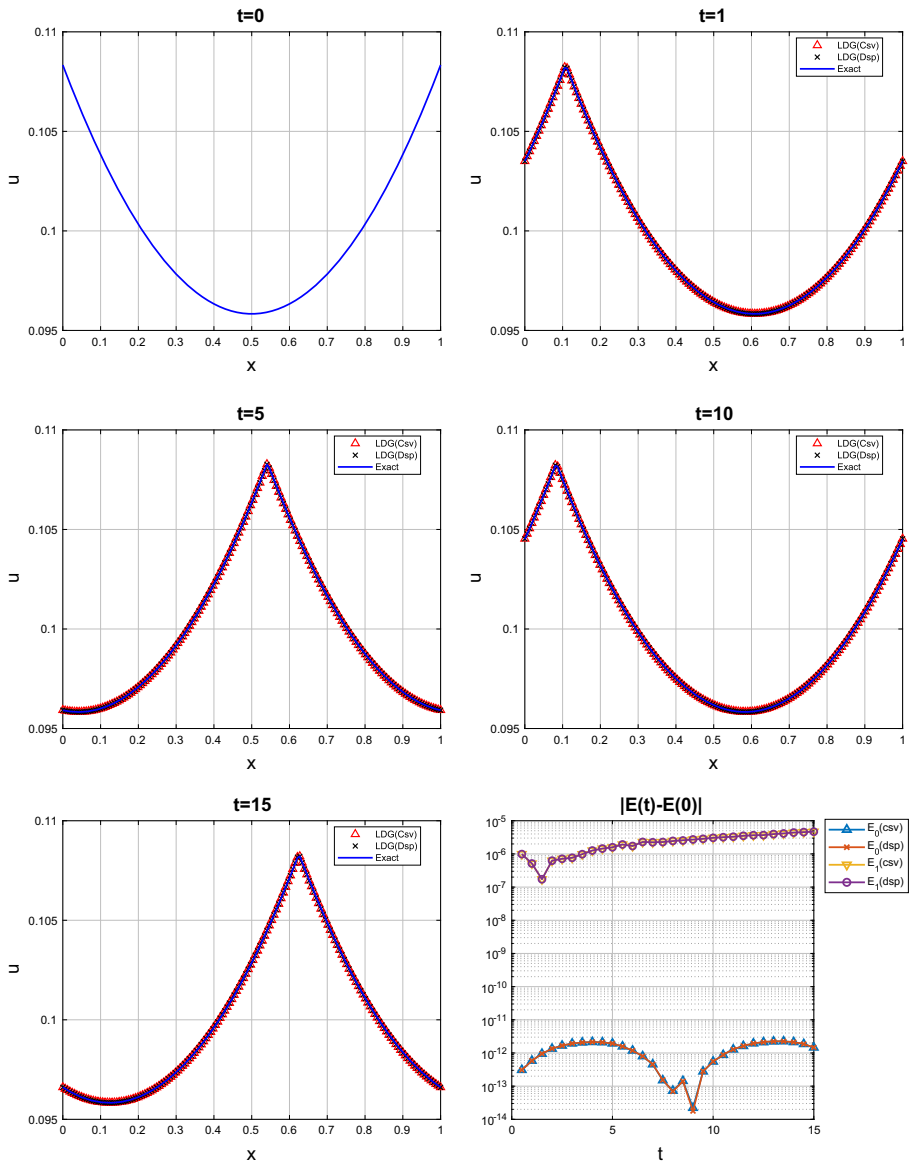
Fig. 1 The one-peakon profiles and evolution $E_0(u_h)$ and $E_1(u_h)$ of the μCH equation. Periodic boundary condition in [0, 1]. P^4 elements and uniform mesh with $N = 160$ cells

0, 1, 5, 10, 15 are showed. The evolution of two Hamiltonian invariants, $E_0(u_h)$ and $E_1(u_h)$, of the μCH equation is also displayed with $t \in [0, 15]$. It illustrates that the moving peaks interaction can be described well by our numerical methods, and both the invariants can keep conservative in the time evolution.
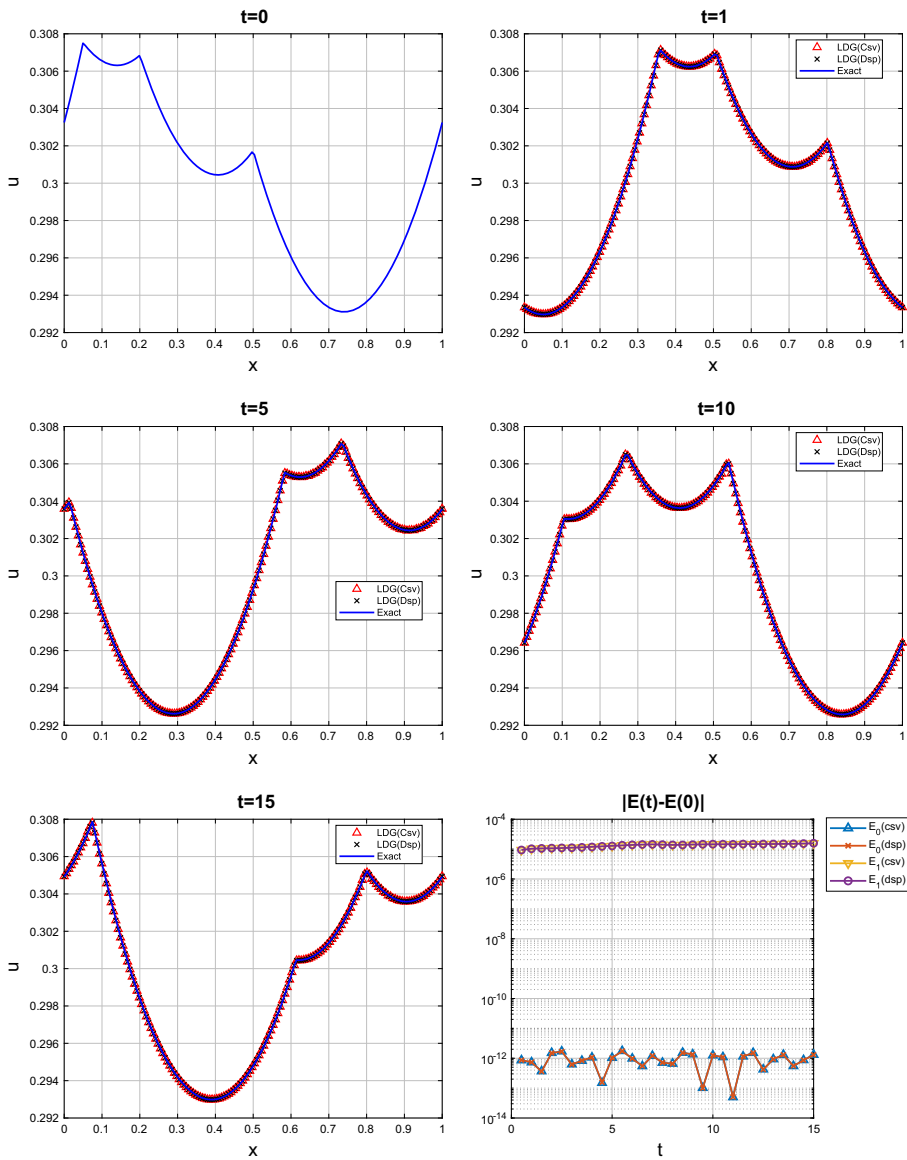
Fig. 2 The three-peakons interaction, evolution of $E_0(u_h)$ and $E_1(u_h)$ of the μCH equation. Periodic boundary condition in $[0, 1]$. P^4 elements and uniform mesh with $N = 160$ cells

5.2 The μDP Equation

In this part, we turn to test the conservative and dissipative schemes for the μDP equation (4.1)

$$u_t + uu_x + 3\mu(u)(A_\mu^{-1}u)_x = 0,$$

Table 2 Example 5.4, accuracy test for the μDP equation with sufficiently smooth solution

N	Dissipative scheme				Conservative scheme			
	L^2 error	Order	L^∞ error	Order	L^2 error	Order	L^∞ error	Order
P^0								
11	2.0643e−01	–	3.4413e−01	–	2.3220e−02	–	3.4064e−02	–
21	1.3454e−01	0.6177	2.3035e−01	0.5791	7.7197e−03	1.5888	1.3505e−02	1.3348
41	7.8905e−02	0.7698	1.3865e−01	0.7324	2.2120e−03	1.8032	4.1389e−03	1.7062
81	4.3135e−02	0.8712	7.6670e−02	0.8547	5.8370e−04	1.9220	1.1339e−03	1.8679
161	2.2618e−02	0.9314	4.0385e−02	0.9248	1.4897e−04	1.9702	2.9178e−04	1.9584
P^1								
11	7.7703e−03	–	2.8610e−02	–	–	–	–	–
21	2.0347e−03	1.9332	6.8873e−03	2.0545	–	–	–	–
41	5.1009e−04	1.9960	2.0135e−03	1.7742	–	–	–	–
81	1.2807e−04	1.9938	5.4600e−04	1.8827	–	–	–	–
161	3.2177e−05	1.9928	1.4075e−04	1.9558	–	–	–	–
P^2								
11	7.0388e−04	–	3.7383e−03	–	1.7134e−03	–	6.4391e−03	–
21	9.4531e−05	2.8965	4.8204e−04	2.9552	9.9294e−05	4.1090	3.9912e−04	4.0120
41	1.2542e−05	2.9141	6.4311e−05	2.9060	1.2450e−05	2.9956	5.5058e−05	2.8578
81	1.6200e−06	2.9526	8.2482e−06	2.9629	1.6044e−06	2.9560	1.0268e−05	2.4228
161	2.0600e−07	2.9753	1.0503e−06	2.9732	2.0091e−07	2.9974	1.4368e−06	2.8372
P^3								
11	4.3209e−05	–	3.3676e−04	–	–	–	–	–
21	3.3349e−06	3.6956	2.6061e−05	3.6918	–	–	–	–
41	2.3286e−07	3.8401	2.0015e−06	3.7027	–	–	–	–
81	1.5264e−08	3.9313	1.3211e−07	3.9212	–	–	–	–
161	1.0326e−09	3.8858	8.6995e−09	3.9247	–	–	–	–

Uniform meshes with N cells at time $t = 0.5$

As we discussed previously, the essential differences between these two schemes are the choices of numerical fluxes, as described in (4.10) and (4.11), respectively. We firstly devote to verify the accuracy of both schemes. Then we apply several examples to verify their capability on the multi-peakons and multi-shocks solutions.

Example 5.4 Smooth periodic waves for μDP

For the lack of smooth travelling examples for the μDP equation, we just use the smooth initial condition as described in Example 5.1 to start evolving our numerical schemes for the μDP equation. Here we take the parameters as before and apply the same skills to get a high-precision numerical solution of the ODE (5.8). We apply the piecewise P^4 polynomial, the uniform mesh with $N = 321$ cells and the fourth-order TVD Runge–Kutta method with the CFL number 0.05 in the dissipative scheme to get a sufficiently accurate numerical simulation, which is regarded as a reference solution to the μDP equation in the process of error computations. The L^2 and L^∞ errors and orders of accuracy for both schemes, at time $t = 0.5$ are showed in Table 2. The periodic boundary conditions and uniform
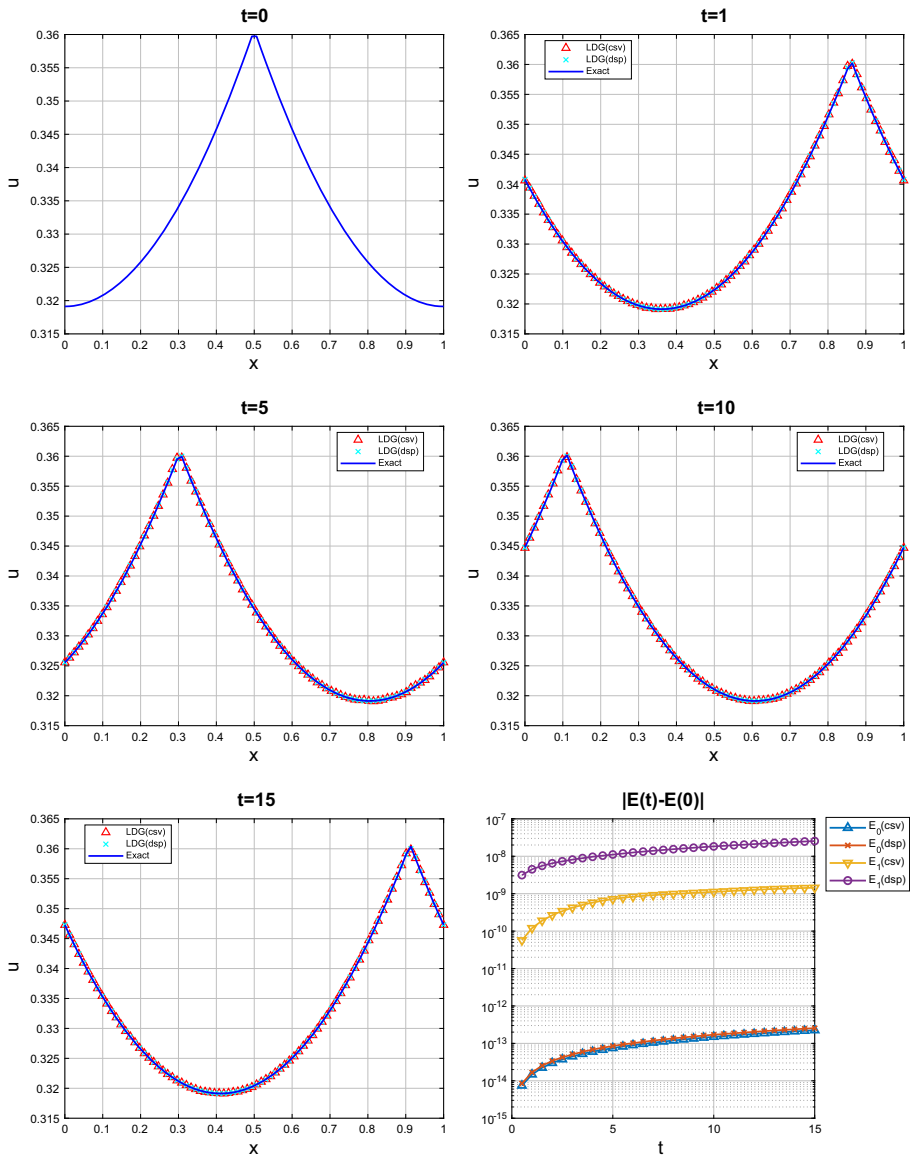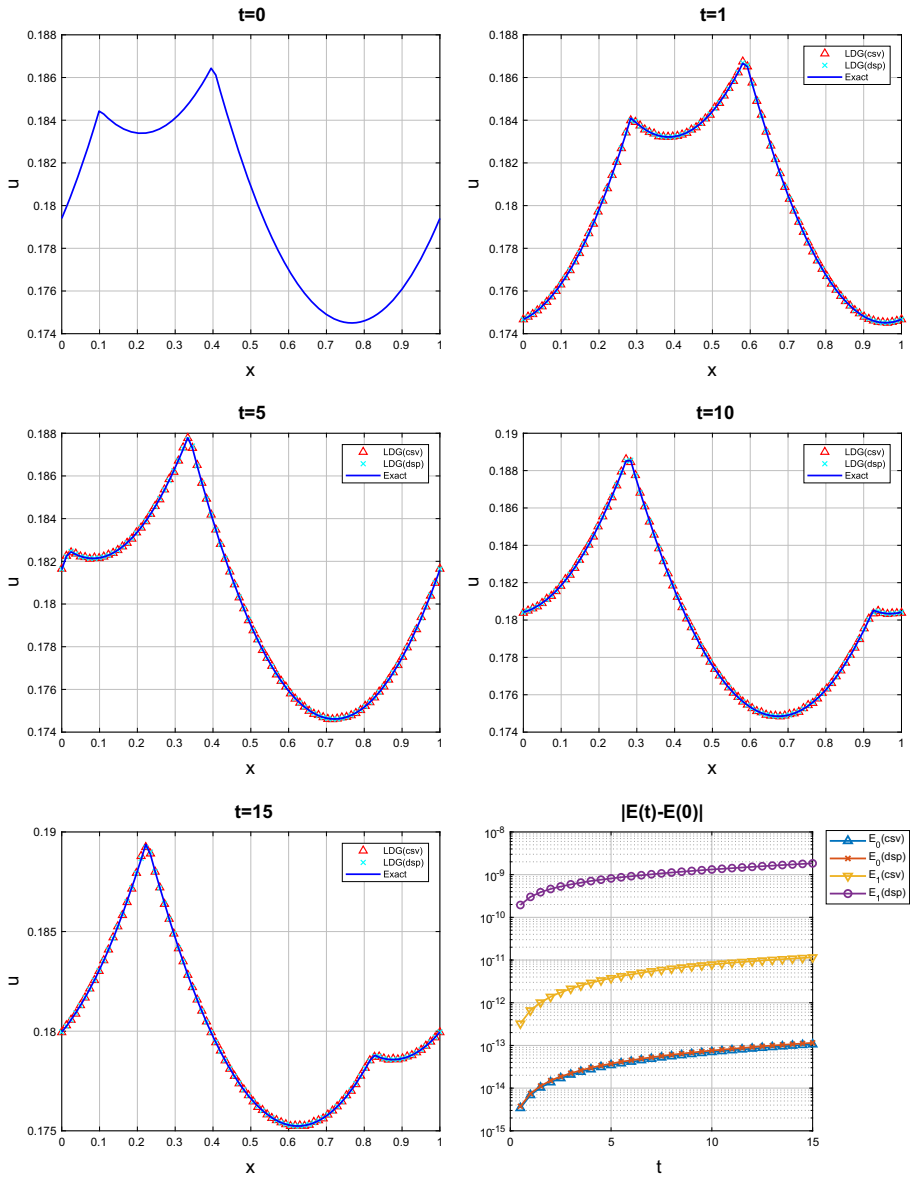
Fig. 3 The evolution of one-peakon solution for the μDP equation with initial data (5.11). Periodic boundary condition in $[0, 1]$. P^2 elements and uniform mesh with $N = 81$ cells

meshes are used in the implementation of both methods. The numerical results verify that the dissipative LDG method for the μDP equation obtains the optimal order of accuracy, which is better than the suboptimal order of accuracy $k + \frac{1}{2}$ as illustrated in Theorem 4.34. It is also found that the conservative scheme of P^0 case achieves some superconvergence than expected. However, the desired results of the conservative scheme are only obtained with restrictions on the parity of order of P^k polynomial (k is even) and number of cells (N is odd), which are assumptions declared in the error estimates for the conservative scheme

Fig. 4 The interaction of two-peakon solution for the μDP equation with initial data (5.12). Periodic boundary condition in [0, 1]. P^2 elements and uniform mesh with $N = 81$ cells

in (4.35). In the process of implementation of the conservative scheme, we find the matrix $\mathbf{D} = \mathbf{A}_\mu - \mathbf{B}_q \mathbf{A}^{-1} \mathbf{B}_v$, defined in Algorithm Flowchart 3.1.1, is invertible only in case of k being even and N being odd. So we only display valid results of the conservative scheme in Table 2.
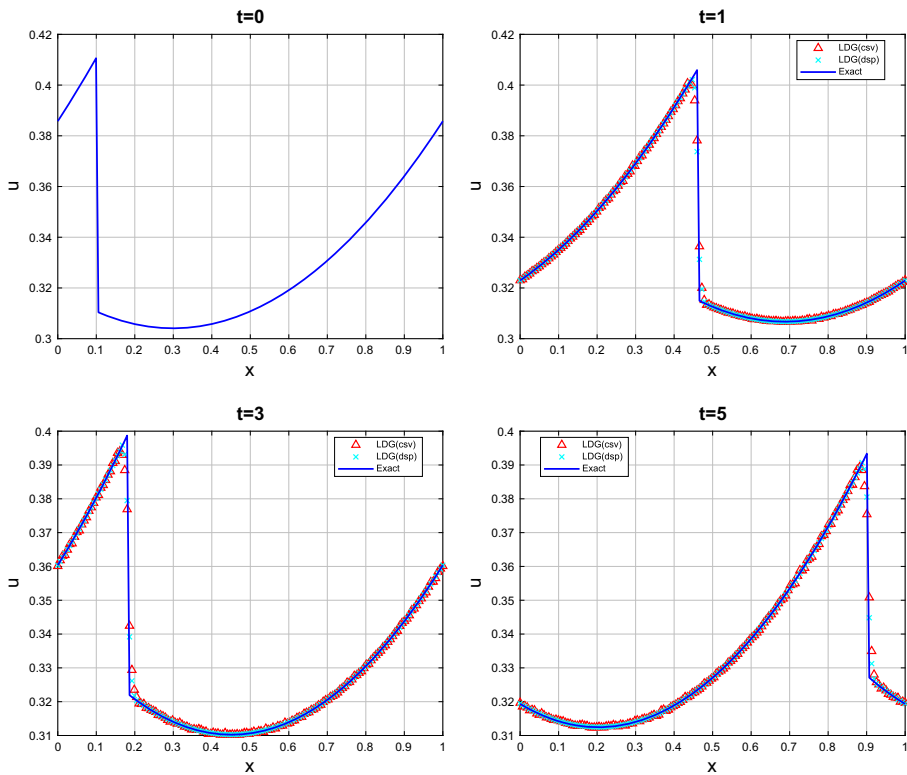
Fig. 5 The profiles of one-shock wave of the μDP equation with initial data (5.13). Periodic boundary condition in [0, 1]. P^2 elements and uniform mesh with $N = 161$ cells

Example 5.5 Peakon solutions for μDP

Now we turn to verify the capability of the two LDG schemes for the μDP equation to simulate the peakon solutions. Initializing the expression we mentioned in (5.1) by setting parameters as follows

$$p_1 = 0.333, \ q^1 = -0.5, \tag{5.11}$$

we get an example for the one-peakon wave of the μDP equation. The numerical simulations with time $t \in [0, 15]$ are depicted in Fig. 3. The evolution of two invariants, $H_0(u_h)$ and $H_1(u_h)$, of the μDP equation is also showed together.

We also apply the initial condition settings as

$$p_1 = 0.1, \ p_2 = 0.08,$$
$$q^1 = 0.4, \ q^2 = 0.1, \tag{5.12}$$

to validate the two-peakons interactive example for the μDP equation. The numerical results and the evolution of $H_0(u_h)$ and $H_1(u_h)$ are depicted in Fig. 4. In both examples, P^2 element, an uniform mesh with $N = 81$ cells and the third order TVD Runge–Kutta method with CFL number 0.1 are utilized. It illustrates that both conservative and dissipative schemes are qualified to simulate the peakon solutions in a long time. And the invariants of u_h keep numerically conservative in both examples.
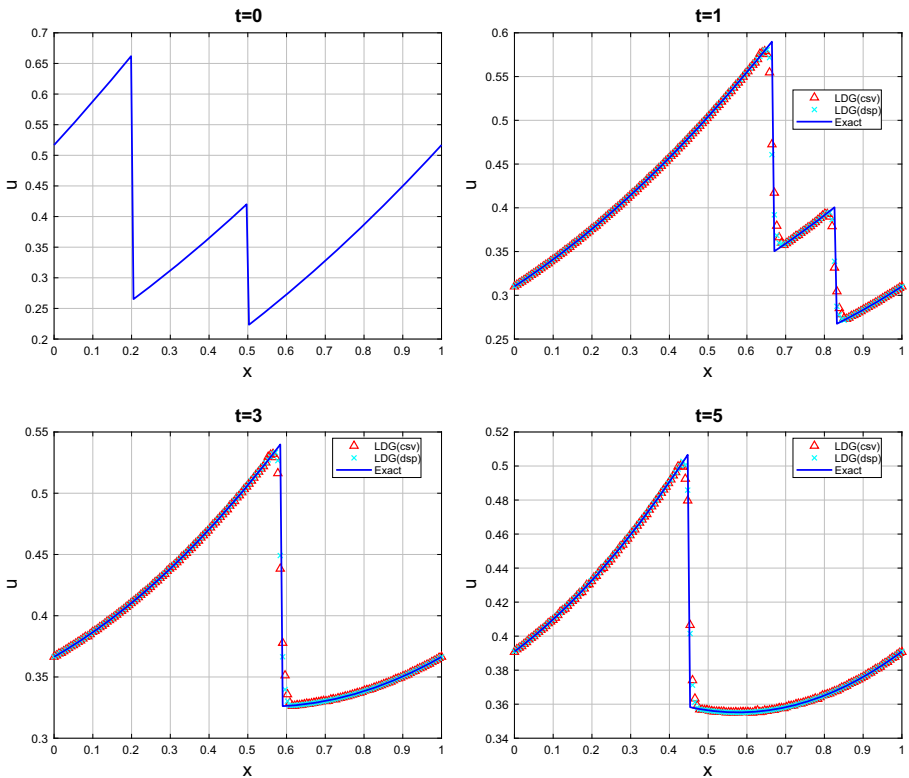
Fig. 6 Interaction of two-shocks solution of the μDP equation with initial data (5.14). Periodic boundary condition in [0, 1]. P^2 elements and uniform mesh with $N = 161$ cells

Example 5.6 Multi-shocks wave solutions for μDP

In this part, we pay attention to the different solutions with multi-shocks for the μDP equation with the initial settings in (5.5) as follows

- One shock

$$p_1(0) = 0.333, \; q^1(0) = 0.1, \; s_1(0) = 0.1, \tag{5.13}$$

- Two shocks

$$p_1(0) = 0.3, \; q^1(0) = 0.2, \; s_1(0) = 0.4,$$
$$p_2(0) = 0.1, \; q^2(0) = 0.5, \; s_2(0) = 0.2, \tag{5.14}$$

- Three shocks

$$p_1(0) = 1, \; q^1(0) = 0.1, \; s_1(0) = 0.12,$$
$$p_2(0) = 0.8, \; q^2(0) = 0.5, \; s_2(0) = 0.8,$$
$$p_3(0) = 0.12, \; q^3(0) = 0.4, \; s_3(0) = 0.2. \tag{5.15}$$

Implement the conservative and dissipative schemes to solve the μDP equation with these three initial conditions successively, then we can obtain the respective simulations displayed in Figs. 5, 6 and 7. Other information about simulations is gathered as follows: the domain
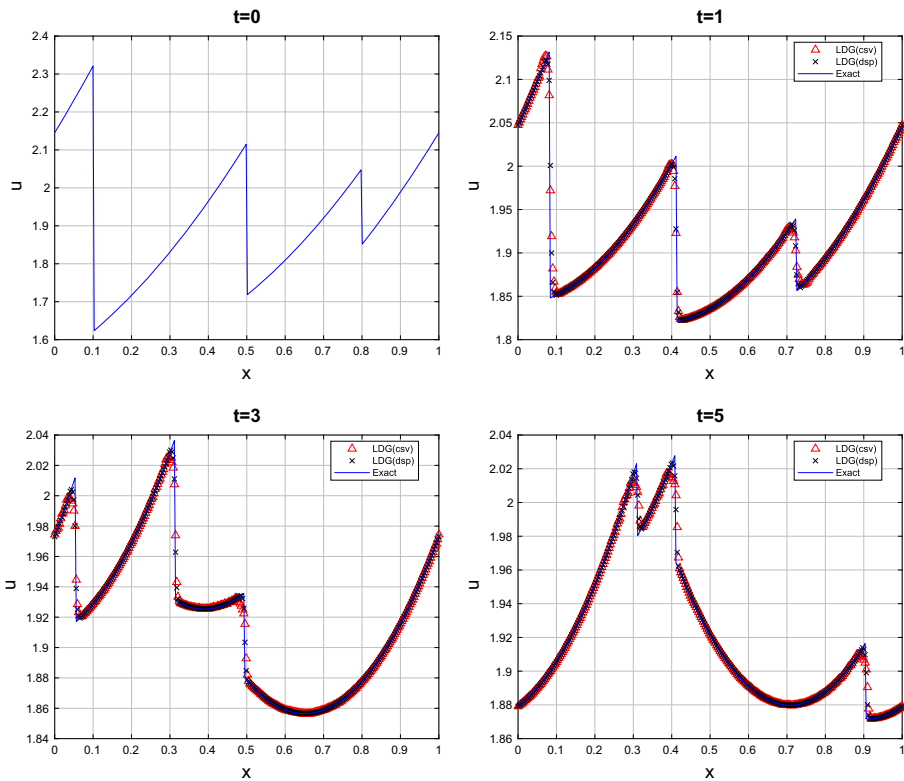
Fig. 7 Interaction of three-shocks solution of the μDP equation with initial data (5.15). Periodic boundary condition in [0, 1]. P^2 elements and uniform mesh with $N = 321$ cells

[0, 1], the P^2 piecewise element and the third order TVD Runge–Kutta method with CFL number 0.1. And we use $N = 161$ cells of uniform mesh for the one-shock and two-shocks waves, yet a more refined mesh with $N = 321$ cells are applied for the three-shocks solution. The TVB limiter in [6] is adopted to modify the shock solutions. In the experiments of one-shock and two-shocks waves, the conservative and dissipative schemes simulate well for the μDP equation. But for the three-shocks solution, the dissipative scheme performs slightly better than the conservative one.

6 Conclusion

In this paper, we have developed a series of LDG schemes, including the conservative and dissipative ones, for both the μ-Camassa–Holm and μ-Degasperis–Procesi equations. The conservation of the Hamiltonian invariants for each equation has been analyzed and a priori error estimates for the schemes have also been given. Several numerical examples in different circumstances were shown to illustrate the accuracy and capability of these LDG schemes. Besides, these LDG schemes inherit the nice properties of DG methods on the flexibility for general geometry meshes, the hp-adaptivity, and excellent parallel efficiency. The LDG method possesses a good potential in solving the μ-version equations and other similar problems.

A Appendix

A.1 Proof of the Equivalence of (1.2) and (1.11)

Proof Notice that

$$(A_\mu u)_t = \mu(u)_t - u_{xxt}$$

and

$$A_\mu \left(\left(\frac{1}{2} u^2 \right)_x \right) = -\frac{1}{2}(u^2)_{xxx} = -3u_x u_{xx} - u u_{xxx}$$

due to the periodicity, then (1.2) can be rewritten as

$$A_\mu(u_t) + A_\mu(uu_x) + 3\mu(u)u_x = 0.$$

Apply the invertible operator A_μ^{-1} to above equation and take into consideration of $\mu(u)$ being a conservative quantity, then we have

$$u_t + uu_x + 3\mu(u)A_\mu^{-1}(u_x) = 0.$$

Comparing the above equation and our desired (1.11), it remains to check the following claim:

$$A_\mu^{-1}(u_x) = (A_\mu^{-1}u)_x.$$

Set $v = A_\mu^{-1}u$, in other word, $u = A_\mu v = \mu(v) - v_{xx}$. v is obviously periodic like u and we know that $\mu(v) = \mu(u)$, which means that $\mu(v)$ is also a conservative quantity. On account of the periodicity and conservation, the mean value $\mu(v) = \int_0^1 v dx$ is a constant no matter where and when, so we have $\mu(v)_x = 0$; furthermore, owing to the periodicity, we also get $\mu(v_x) = 0$.

Now we apply A_μ to $A_\mu^{-1}(u_x) - (A_\mu^{-1}u)_x$, then

$$
\begin{aligned}
& A_\mu A_\mu^{-1}(u_x) - A_\mu(A_\mu^{-1}u)_x \\
&= u_x - A_\mu(v_x) \\
&= (A_\mu v)_x - A_\mu(v_x) \\
&= (\mu(v)_x - (v_{xx})_x) - (\mu(v_x) - (v_x)_{xx}) \\
&= \mu(v)_x - \mu(v_x) \\
&= 0.
\end{aligned}
$$

Thus we have proven the claim, and further completed the equivalence of (1.11) and (1.2). $\qquad\square$

A.2 Proof of Lemma 3.7

Proof By the Proposition 3.2, we know

$$\mu(u_h)_t = 0.$$

Then by the orthogonality of L^2 projection,

$$s^e = (\mathcal{P}^+ u - u) \perp \mathbb{P}^{k-1},$$

so

$$\int_I s^e \cdot 1 dx = 0.$$

Then we can get $\mu(s^e) = \mu(\mathcal{P}^+ u) - \mu(u) = 0$. In addition to the fact $\mu(u)_t = 0$, we have

$$\mu(\mathcal{P}^+ u)_t = 0.$$

Taking consideration of the definitions of s and s^e, we easily get

$$\frac{d}{dt}\mu(s) \equiv 0, \quad \frac{d}{dt}\mu(s^e) \equiv 0.$$

$\square$

A.3 Proof of Lemma 3.8

Proof

$$\sum_{j=1}^{N} \mathcal{B}_j(s - s^e, \xi - \xi^e, v - v^e, \delta - \delta^e; -s, \delta_t, s, -\delta, v)$$

$$= \sum_{j=1}^{N} \mathcal{B}_j(s, \xi, v, \delta; -s, \delta_t, s, -\delta, v) - \sum_{j=1}^{N} \mathcal{B}_j(s^e, \xi^e, v^e, \delta^e; -s, \delta_t, s, -\delta, v) \quad \text{(A.1)}$$

By the same argument as that used for the stability in Proposition 3.2 and on account of the results in Lemma 3.7, the first term of the right-hand side in (A.1) becomes

$$\mathcal{B}_j(s, \xi, v, \delta; -s, \delta_t, s, -\delta, v) = \int_{I_j} (\delta_t \delta) dx + \Psi_{j+\frac{1}{2}} - \Psi_{j-\frac{1}{2}},$$

where $\Psi = v^- s^- - \widehat{v} s^- - \widecheck{s} v^- + \delta_t^- s^- - \widehat{\delta_t} s^- - \widehat{s} \delta_t^-$.

As to the second term of the right-hand side in (A.1), we have

$$\mathcal{B}_j(s^e, \xi^e, v^e, \delta^e; -s, \delta_t, s, -\delta, v)$$

$$= \int_{I_j} \delta^e \delta_t dx + \int_{I_j} (\delta^e v - v^e \delta) dx + \int_{I_j} (\delta_t^e s_x + s^e (\delta_t)_x + v^e s_x + s^e v_x) dx$$

$$+ \left((\widehat{v^e} + \widehat{\delta_t^e})[s] \right)_{j-\frac{1}{2}} + \left(\widehat{s^e}[\delta_t] \right)_{j-\frac{1}{2}} + \left(\widecheck{s^e}[v] \right)_{j-\frac{1}{2}} + \Phi_{j+\frac{1}{2}} - \Phi_{j-\frac{1}{2}}, \quad \text{(A.2)}$$

where $\Phi = \widehat{v^e} s^- - \widecheck{s^e} v^- - \widehat{\delta_t^e} s^- - \widehat{s^e} \delta_t^-$. Because $\mathcal{P}$ is a local L^2 projection, and $\mathcal{P}^+$, although not a local L^2 projection, does have the property that $s - \mathcal{P}^+ s$ is locally orthogonal to all polynomials of degree up to $k - 1$, we have

$$\int_{I_j} \delta^e \delta_t dx + \int_{I_j} (\delta^e v - v^e \delta) dx + \int_{I_j} (\delta_t^e s_x + s^e (\delta_t)_x + v^e s_x + s^e v_x) dx = 0.$$

Noticing the special interpolation property of the projection $\mathcal{P}^+$, we have

$$(\widehat{s^e}[\delta_t])_{j-\frac{1}{2}} + (\widecheck{s^e}[v])_{j-\frac{1}{2}} = 0.$$

Then equation (A.2) becomes

$$\mathcal{B}_j(s^e, \xi^e, v^e, \delta^e; -s, \delta_t, s, -\delta, v) = \left((\widehat{v^e} + \widehat{\delta_t^e})[s] \right)_{j-\frac{1}{2}} + \Phi_{j+\frac{1}{2}} - \Phi_{j-\frac{1}{2}}.$$

Combining the above equation with (A.1), summing over j, taking into account the periodic boundary condition, we obtain the desired equality (3.47). □

A.4 Proof of Lemma 3.9

For the proof of this lemma, we follow the idea of Lemma 3.4 and 3.5 in [19]. For $f(u) = 2\mu(u)u$ in the μCH equation (1.1), we have $f''(u) = 0$ and $f'''(u) = 0$, then we could simplify the proof.

Proof Review the equality (3.48), and the estimates for every part in the right-hand side of (3.48) is as following

- **Conservative scheme**

For the last term, if $\widehat{f}$ is chosen as (3.14), we get trivially

$$\sum_{j=1}^{N} \left(\left(f(\{u_h\}) - \widehat{f} \right)[s] \right)_{j+\frac{1}{2}} = 0,$$

for the reason that $\widehat{f} = \frac{1}{2} \left(f(u_h^+) + f(u_h^-) \right) = 2\mu_0(u_h^- + u_h^+) = f(\{u_h\})$.

- **Dissipative scheme**

Besides, when $\widehat{f}$ is chosen as the Lax-Friedrichs flux (3.15), via the fact $[u_h] = [u_h - u] = [s^e - s]$, we have

$$\sum_{j=1}^{N} \left(\left(f(\{u_h\}) - \widehat{f} \right)[s] \right)_{j+\frac{1}{2}} = \frac{\alpha}{2} \sum_{j=1}^{N} ([u_h][s])_{j+\frac{1}{2}}$$

$$= \frac{\alpha}{2} \sum_{j=1}^{N} ([s^e][s])_{j+\frac{1}{2}} - \frac{\alpha}{2} \sum_{j=1}^{N} ([s][s])_{j+\frac{1}{2}}$$

$$\leq -\frac{\alpha}{2} \sum_{j=1}^{N} ([s]^2)_{j+\frac{1}{2}} + Ch^{2k+1},$$

where $\alpha = \max_{u_h} |f'(u_h)| \geq 0$.

For the other two terms $\sum_{j=1}^{N} \int_{I_j} (f(u) - f(u_h))s_x dx + \sum_{j=1}^{N} (f(u_h) - f(\{u_h\}))[s])_{j+\frac{1}{2}}$, observing that $f(u) = 2\mu(u)u$ where $\mu(u)$ is conservative, denoting $C_\mu = 2\mu(u)$, we can obtain

$$f(u) - f(u_h) = C_\mu(s - s^e),$$
$$f(u) - f(\{u_h\}) = C_\mu(\{s\} - \{s^e\}),$$

then

$$\sum_{j=1}^{N} \int_{I_j} (f(u) - f(u_h))s_x dx + \sum_{j=1}^{N} (f(u_h) - f((\{u_h\}))[s])_{j+\frac{1}{2}}$$

$$= \sum_{j=1}^{N} \int_{I_j} C_\mu s s_x dx + \sum_{j=1}^{N} C_\mu(\{s\}[s])_{j+\frac{1}{2}} - \left(\sum_{j=1}^{N} \int_{I_j} C_\mu s^e s_x dx + \sum_{j=1}^{N} C_\mu(\{s^e\}[s])_{j+\frac{1}{2}} \right)$$

$$= \mathscr{T}_1 + \mathscr{T}_2,$$

where

$$\mathscr{T}_1 = \sum_{j=1}^{N} \int_{I_j} C_\mu s s_x dx + \sum_{j=1}^{N} C_\mu (\{s\}[s])_{j+\frac{1}{2}},$$

$$\mathscr{T}_2 = -\left(\sum_{j=1}^{N} \int_{I_j} C_\mu s^e s_x dx + \sum_{j=1}^{N} C_\mu (\{s^e\}[s])_{j+\frac{1}{2}} \right).$$

Making further analysis, we can get

$$\mathscr{T}_1 = C_\mu \left(\sum_{j=1}^{N} \int_{I_j} \frac{1}{2}(s^2)_x dx + \sum_{j=1}^{N} \left(\frac{s^+ + s^-}{2} (s^+ - s^-) \right)_{j+\frac{1}{2}} \right) = 0,$$

$$\mathscr{T}_2 = -C_\mu \left(\sum_{j=1}^{N} \int_{I_j} s^e s_x dx + \sum_{j=1}^{N} (\{s^e\}[s])_{j+\frac{1}{2}} \right)$$

$$\leq C_\mu \|s^e\| \|s_x\| + C_\mu \|s^e\|_{\Gamma_h} \|s\|_{\Gamma_h}$$

$$\leq C \|s\|^2 + C h^{2k}.$$

Combining them and we can get the conclusion of Lemma 3.9

$$\sum_{j=1}^{N} \mathcal{H}_j(f; u, u_h; s) \leq C \|s\|^2 + C h^{2k}.$$

$\square$

References

1. Bassi, F., Rebay, S.: A high-order accurate discontinuous finite element method for the numerical solution of the compressible Navier–Stokes equations. J. Comput. Phys. **131**(2), 267–279 (1997)
2. Bona, J., Chen, H., Karakashian, O., Xing, Y.: Conservative, discontinuous Galerkin-methods for the generalized Korteweg-de Vries equation. Math. Comput. **82**(283), 1401–1432 (2013)
3. Brenner, S., Scott, R.: The Mathematical Theory of Finite Element Methods, vol. 15. Springer, Berlin (2007)
4. Chen, R.M., Lenells, J., Liu, Y.: Stability of the μ-Camassa–Holm peakons. J. Nonlinear Sci. **23**(1), 97–112 (2013)
5. Ciarlet, P.G.: The Finite Element Method for Elliptic Problems. SIAM, Philadelphia (2002)
6. Cockburn, B., Shu, C.-W.: TVB Runge–Kutta local projection discontinuous Galerkin finite element method for conservation laws. II. General framework. Math. Comput. **52**(186), 411–435 (1989)
7. Cockburn, B., Shu, C.-W.: The local discontinuous Galerkin method for time-dependent convection-diffusion systems. SIAM J. Numer. Anal. **35**(6), 2440–2463 (1998)
8. Gottlieb, S., Shu, C.-W., Tadmor, E.: Strong stability-preserving high-order time discretization methods. SIAM Rev. **43**(1), 89–112 (2001)
9. Karakashian, O., Xing, Y.: A posteriori error estimates for conservative local discontinuous Galerkin methods for the generalized Korteweg–de Vries equation. Commun. Comput. Phys. **20**(1), 250–278 (2016)
10. Khesin, B., Lenells, J., Misiołek, G.: Generalized Hunter–Saxton equation and the geometry of the group of circle diffeomorphisms. Math. Ann. **342**(3), 617–656 (2008)
11. Lenells, J., Misiołek, G., Tığlay, F.: Integrable evolution equations on spaces of tensor densities and their peakon solutions. Commun. Math. Phys. **299**(1), 129–161 (2010)
12. Liu, H., Xing, Y.: An invariant preserving discontinuous Galerkin method for the Camassa–Holm equation. SIAM J. Sci. Comput. **38**(4), A1919–A1934 (2016)

13. Meng, X., Shu, C.-W., Wu, B.: Optimal error estimates for discontinuous Galerkin methods based on upwind-biased fluxes for linear hyperbolic equations. Math. Comput. **85**(299), 1225–1261 (2016)
14. Shu, C.-W., Osher, S.: Efficient implementation of essentially non-oscillatory shock-capturing schemes. J. Comput. Phys. **77**(2), 439–471 (1988)
15. Wang, H., Shu, C.-W., Zhang, Q.: Stability and error estimates of local discontinuous galerkin methods with implicit–explicit time-marching for advection–diffusion problems. SIAM J. Numer. Anal. **53**(1), 206–227 (2015)
16. Xia, Y.: Fourier spectral methods for Degasperis–Procesi equation with discontinuous solutions. J. Sci. Comput. **61**(3), 584–603 (2014)
17. Xia, Y., Xu, Y.: Weighted essentially non-oscillatory schemes for Degasperis–Procesi equation with discontinuous solutions. Ann. Math. Sci. Appl. **2**(2), 319–340 (2017)
18. Xu, Y., Shu, C.-W.: Local discontinuous Galerkin methods for two classes of two-dimensional nonlinear wave equations. Physica D Nonlinear Phenom. **208**(1–2), 21–58 (2005)
19. Xu, Y., Shu, C.-W.: Error estimates of the semi-discrete local discontinuous Galerkin method for nonlinear convection-diffusion and KdV equations. Comput. Methods Appl. Mech. Eng. **196**(37), 3805–3822 (2007)
20. Xu, Y., Shu, C.-W.: A local discontinuous Galerkin method for the Camassa–Holm equation. SIAM J. Numer. Anal. **46**(4), 1998–2021 (2008)
21. Xu, Y., Shu, C.-W.: Local discontinuous Galerkin method for the Hunter–Saxton equation and its zero-viscosity and zero-dispersion limits. SIAM J. Sci. Comput. **31**(2), 1249–1268 (2008)
22. Xu, Y., Shu, C.-W.: Dissipative numerical methods for the Hunter–Saxton equation. J. Comput. Math. **28**, 606–620 (2010)
23. Xu, Y., Shu, C.-W.: Local discontinuous Galerkin methods for high-order time-dependent partial differential equations. Commun. Comput. Phys. **7**(1), 1 (2010)
24. Xu, Y., Shu, C.-W.: Local discontinuous Galerkin methods for the Degasperis–Procesi equation. Commun. Comput. Phys. **10**(2), 474–508 (2011)
25. Yan, J., Shu, C.-W.: A local discontinuous Galerkin method for KdV type equations. SIAM J. Numer. Anal. **40**(2), 769–791 (2002)
26. Zhang, Q., Shu, C.-W.: Error estimates to smooth solutions of Runge–Kutta discontinuous Galerkin methods for scalar conservation laws. SIAM J. Numer. Anal. **42**(2), 641–666 (2004)
27. Zhang, Q., Xia, Y.: Conservative and dissipative local discontinuous Galerkin methods for Korteweg–de Vries type equations. Commun. Comput. Phys. **25**(3), 532–563 (2019)